SNS-101060100-TR0004-R00

Summary of Mercury Target Pitting Issue

Date: April 2002

A U.S. Department of Energy Multilaboratory Project

SPALLATION NEUTRON SOURCE

Argonne National Laboratory • Brookhaven National Laboratory • Thomas Jefferson National Accelerator Facility • Lawrence Berkeley National Laboratory • Los Alamos National Laboratory • Oak Ridge National Laboratory

SNS-101060100-TR0004-R00

Summary of Mercury Target Pitting Issue

**J. R. Haines, K. Farrell, J. D. Hunn, D. C. Lousteau, L.K. Mansur,
T. J. McManamy, S. J. Pawel, and B. W. Riemer**

April 1, 2002

Date Published: April 2002

Prepared for the
U.S. Department of Energy
Office of Science

UT-BATTELLE, LLC
managing the
Spallation Neutron Source Activities at the
Argonne National Laboratory
Brookhaven National Laboratory
Thomas Jefferson National Accelerator Facility
Lawrence Berkeley National Laboratory
Los Alamos National Laboratory
Oak Ridge National Laboratory
under contract DE-AC05-00OR22725
for the
U.S. DEPARTMENT OF ENERGY

Table of Contents

List of Tables

List of Figures

Executive Summary

A team of researchers from the Japan Atomic Energy Research Institute (JAERI) reported in the fall of 2000 that they had discovered pitting damage on stainless steel surfaces in contact with mercury that was subjected to mechanically induced pressure pulses of the magnitude expected in short-pulse spallation targets. Because of concerns that pitting damage might also occur in the stainless steel container for the SNS mercury target, the SNS target development team conducted tests at Los Alamos National Laboratory's (LANL) Weapons Neutron Research (WNR) facility during July 2001. Cylindrically shaped, mercury-filled containers with flat end caps were irradiated with 200 pulses of 800 MeV protons at relevant beam intensities. Test results showed that, at least for the materials and target configurations tested, pitting damage occurred for beam intensities comparable to SNS operation at almost 3 MW. A cluster of large pits, visible to the naked eye, as well as smaller, more randomly distributed pits were seen in micrograph images of all four window specimens used in the July 2001 tests. Although a cluster of large pits was also found on the surface hardened (Kolsterising, a carburizing process), annealed 316SS window, dramatically fewer randomly distributed pits could be detected at the resolution used to perform the inspections (~ 5 μm), thus giving some indication that hardening reduces the degree of pitting.

The magnitude of the pressure pulse, results of off-line cavitation threshold tests, and post-test examination of damaged surfaces, lead us to conclude with a reasonably large degree of confidence that the mechanism causing the pitting damage is collapse of bubbles created as part of a mercury cavitation process. Because of this, the cavitation damage literature has been studied to help understand the phenomenon and postulate potential solutions or improvements.

Considering the July 2001 test results, it was concluded that additional testing was needed to further examine the pitting phenomenon and investigate possible solutions, or at least reductions, to the pitting problem. With this in mind, tests on an array of targets were conducted in December 2001 at the WNR facility. Four mercury targets, using different cross-sectional shapes or different window materials, were exposed to 200 beam pulses. Most notably, a target with a rectangular cross section was used in an attempt to eliminate the postulated radial focusing of the pressure wave and to represent a shape that was more prototypical of the actual SNS target shape. This target also included a double wall, forming a thin mercury layer in an attempt to simulate the window cooling geometry used in the baseline SNS target design. Post-irradiation examination of the targets irradiated in December has begun and is scheduled for completion in April 2002. The present version of this report does not incorporate results from the December 2001 tests. When results become available, they will be added.

Estimating the target lifetime using the data from the 200 pulse tests requires an enormous extrapolation, i.e., by more than a factor of one million. Assumptions regarding the nature of the pitting process that have yet to be validated are required to create this erosion lifetime estimate. Nonetheless, linear extrapolations have been performed to give some comparison of projected lifetimes to design goals. These estimates illustrate that the large cluster of pits near the center of the beam interaction region must be eliminated to achieve an adequate target lifetime. If the large pits are eliminated by geometric or other considerations (not fully demonstrated yet), bare 316SS should be adequate for the planned first six months of low power operation with no target replacement. In addition, if we can find a target container material that has an erosion resistance comparable to that of the Kolsterised surface (limited to 33 μm thickness) with an erosion thickness greater than 500 μm, then lifetimes approaching 1/3 of the goal of 1250 hours at 2 MW

operation may be possible. This would give us adequate target lifetime for the first several years of operation, when power levels are being slowly increased. This initial operating period could be used to further understand the problem and examine methods to extend the erosion lifetime. It should be noted that there is risk associated with this approach, that is, if an adequate mercury target lifetime is not ultimately achieved, changing from a mercury target to a water-cooled solid target would require considerable downtime (roughly estimated to be 2 years) for the SNS facility.

Finally, the direct relevance of the off-line and in-beam tests conducted so far is somewhat questionable since many of the variables that could be important for pitting damage cannot be accurately simulated in these tests. Several examples of the discrepancies between tests and the actual SNS conditions include:

- Interactions between subsequent beam pulses could be important if the residence time of cavitation bubbles is comparable to or longer than the 17 ms between pulses in SNS (corresponds to 60 Hz repetition rate),
- Flowing of the mercury may alter the contact condition between the mercury and stainless steel and thereby change the way in which bubbles form and collapse,
- The shapes of targets used in tests have been either different or rather great simplifications of the SNS target shape and do not include the long open-ended Hg supply and return lines, and
- Both off-line and in-beam tests have been limited to a small number of pulses (≤ 200) compared to the baseline target lifetime (based on radiation damage) of 2.7×10^8 pulses.

Given the uncertainty in erosion lifetime, it is concluded that more in-beam tests should be performed to examine whether the proposed ideas for target shape and materials can be shown to extrapolate to reasonable lifetimes (say 10^8 pulses, which is equivalent to almost 3 weeks of operation at 60 Hz, for example) at SNS relevant power levels (≥ 1 MW). Tests scheduled for May and June 2002 will examine alternate materials, coatings, target shapes, and power levels, but additional tests may be required. Also, exploring ideas for developing an off-line pitting test apparatus capable of going to a high number of cycles should be pursued since such an apparatus could greatly reduce the uncertainty associated with extrapolating from the 200 in-beam test cycles to the SNS lifetime of 2.7×10^8 cycles. Finally, developing Hg target design concepts, diagnostics, and post-irradiation examination procedures that emphasize the experimental nature of early SNS operations should be pursued.

1.0 Purpose

The purpose of this paper is to summarize relevant information on the so-called pitting issue for the mercury target. With this goal in mind, results of in-beam as well as off-line experiments and computer model predictions are reviewed along with a summary of information from related technical literature. Plans for completion of tests in FY 2002, potential implications of this issue on target design and implementation, and speculation on the most likely physical mechanisms that could explain this phenomenon are also summarized.

2.0 Background/Introduction

One of the most important issues associated with using liquid metals as targets for pulsed proton beams is withstanding the loads caused by the rapid pressure increase resulting from the intense heating of the liquid metal from a single pulse of protons. This heating occurs essentially instantaneously compared to acoustic wave time scales; therefore, the mercury undergoes a large pressure increase. Most of the previous SNS R&D program efforts on this issue had focused on studying the effects that these pressure spikes have on the structural integrity of the mercury target container. For example, in-beam tests with mercury targets conducted prior to 2001 concentrated on measuring the vessel strain using an array of target shapes, diagnostics, and instruments.

During 2000, a team of researchers at the Japan Atomic Energy Research Institute (JAERI) observed pitting of stainless steel surfaces that were in contact with mercury subjected to large mechanically induced pressure pulses of the same magnitude as those expected for full power (2 MW) pulses in SNS. The question then became; “Do the inner surfaces of liquid mercury target containers with comparable beam-induced pressure pulses also pit?” Post-irradiation examinations of targets previously used in pulsed proton beam tests at LANL’s WNR facility were unable to resolve this question because no pre-test inspections had been performed and the roughness of the surfaces was too great to distinguish between beam-induced pits and other imperfections in the surface of the materials.

Because of the urgency associated with completing the SNS target design, two test campaigns were conducted in 2001 to study the pitting issue; the first in July and the second in December. Large pits, visible to the naked eye, were found near the center of all four diaphragms

tested in July 2001. Microscopy revealed that small, randomly distributed pits were also present on the diaphragms, although there were dramatically fewer of these small pits on the diaphragm that had been treated with a surface hardening process. The December 2001 tests were dedicated to further examining the pitting phenomenon and looking at an array of possible solutions, or at least reductions, to the pitting problem. Post-irradiation examination of the targets irradiated in December will be completed in April 2002.

3.0 Summary of Experimental Results

3.1 WNR Tests

3.1.1 Test description

Two test campaigns were conducted at the LANSCE – WNR during 2001 to investigate cavitation damage in mercury spallation targets. Target components from the first of these (tests have been thoroughly examined, while examinations from the second are currently in progress.

The WNR beam parameters are summarized in Table 1. Although total energy per pulse is substantially lower than the SNS target, by tailoring the beam size, maximum energy density in test targets is comparable to that in SNS. Using a test target size that is roughly ½ scale of SNS, the proportion of the beam cross-sectional area to the target cross-sectional area is also comparable.

Two targets were tested in the July campaign. Both of these were the so-called "Large Effects" (LE) type, which is a simple cylindrical shape with a 100 mm diameter (4 inch) and 286 mm (11.4 inch) overall length. The end flanges are flat and have been thinned (~ 1 mm thick) to produce large strains in response to the pressure pulse. Note that the SNS target minimum thickness is 1.25 mm. A sketch of the target geometry on its support stand is shown in Fig. 1.

Table 1. WNR Beam Parameters for Cavitation Damage Tests

	SNS (@ 2 MW)	WNR
Proton Energy [GeV]	1	0.8
Protons per pulse	2×10^{14}	2.8×10^{13}
Beam size [mm]	Elliptic, ~ 70x200	Circular, $\sigma \sim 10$
Energy deposited in mercury target [kJ]	20	2.2
Maximum energy deposition density [MJ/m^3]	13	19

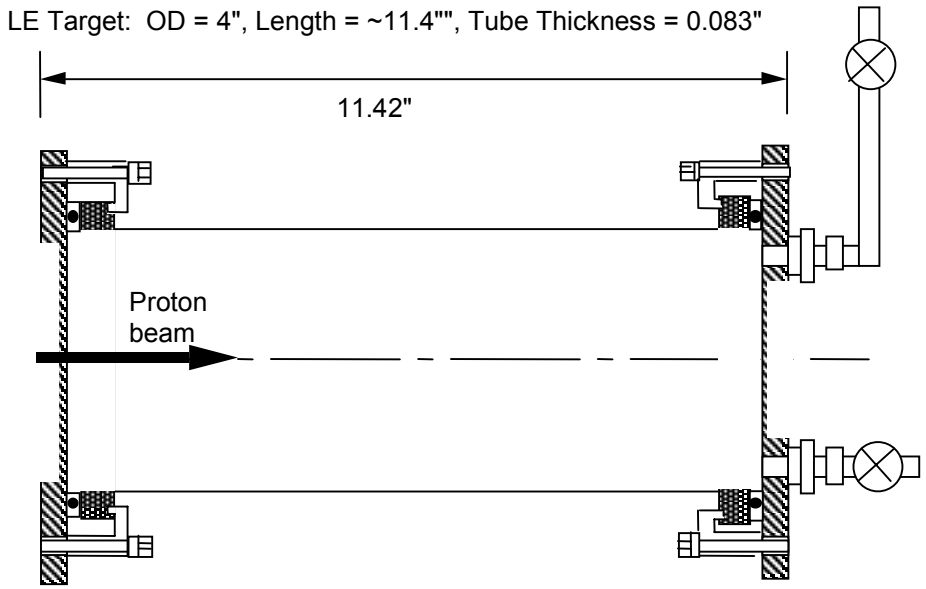

Fig. 1. LE Target Geometry

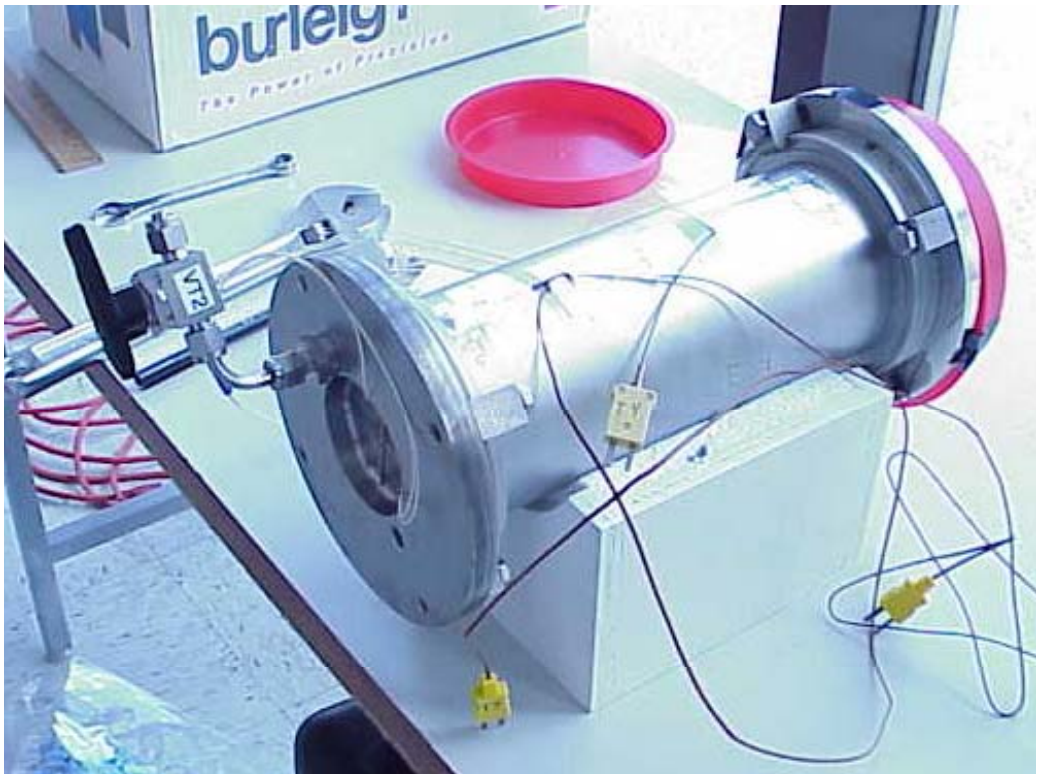

Fig. 2. LE4 Target Before Test

The first of the targets (LE3) used flanges made of 316LN stainless steel. This is the same material to be used in the SNS target; the flanges were also annealed to approximate regions of the target affected by welding that lose cold working. Likewise, the second target (LE4) used annealed 316 LN, but the front flange (up beam) was treated after annealing with a surface hardening process called "Kolsterising," a proprietary low temperature carburizing process. This process increased surface hardness up to 1100 Hv over a depth of roughly 30 μm. Note that the annealed surface hardness was approximately 140 Hv. The only other difference for LE4 was the inclusion of an array of small disk specimens of various materials (10-mm diameter) around the cylinder wall. No pitting was found on any of the specimens, so no further discussion of these specimens is provided in this report. A picture of the LE4 target during pre-test preparation is shown in Fig. 2.

During testing, targets were set in secondary container boxes and positioned to align the axis of the target with the beam. The technique used has limited precision; errors of a few mm are possible. The average location of the beam was determined after testing using activation surveys with a collimating instrument.

In addition to measuring strain on the thinned regions of the flange (membranes), thermocouples monitored the target temperature. Beam pulses were repeated at a maximum rate of one per minute over several sessions until 200 total pulses were achieved. Maximum target temperature was less than 50°C.

3.1.2 Photographs of large pits

After irradiation, the targets were stored at the WNR for about one-month for activation to subside. At that time, the mercury was carefully drained from the targets and they were shipped back to ORNL. Disassembly and decontamination work was conducted in a laboratory at ORNL.

It was immediately apparent that there was damage on all flanges. Clusters of pits near the geometric centers were seen unaided, the clusters ranging from a few to nearly 10 mm in size. Images of the front and rear flanges of LE3 are shown in Fig. 3 and Fig. 4. Scribed "X" marks can be seen at the geometric center; the pit clusters were located a few mm from the centers in all cases. The size of these clusters was larger on front flanges, but the size proportion front to rear did not scale with beam intensity. The beam was nearly stopped in these targets and its intensity at the rear was considerably less than 10% compared to the front.

Activation surveys were conducted on the flanges to locate the (average) beam centers relative to the geometric centers and pit clusters. Fig. 5 shows the result for the front flange of LE3. It can be seen that the while the beam was directly above the geometric center, the high damage region was below by twice the distance. This was true for the LE4 front flange as well. This observation has sprouted theories that the axisymmetric target geometry used for these tests unfortunately focuses reflections off the cylindrical walls leading to intense rarefaction near the axis, and hence more aggressive cavitation. Such theories remain unverified.

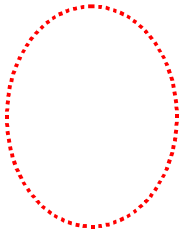

Fig. 3. Front Flange of LE3

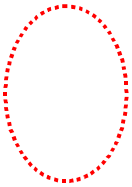

Fig. 4. Rear Flange of LE3

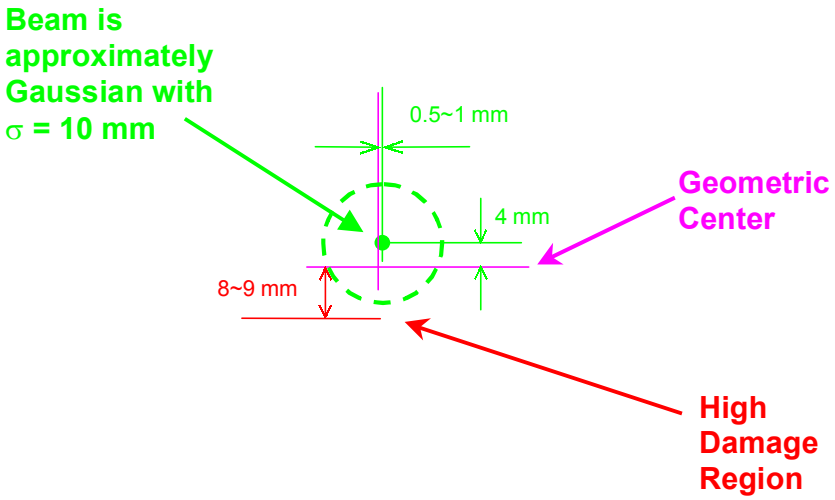

Fig. 5. Average Beam Center on LE3 Front Flange

3.1.3 Detailed Examination

Scanning electron microscopy (SEM), optical microscopy, and laser profilometry have all been used to conduct detailed examination of the flange surfaces before and after irradiation. Flanges were machined flat and highly polished to assist in the identification of any features larger than a few microns that may have been introduced by the test. Flanges were then annealed to remove work hardening introduced by the machining and polishing. The annealing also resulted in a visible grain structure on the polished face, which aided in verification of the position on the flange during microscopy. Polishing was difficult due to the large diameter of the flange, so some areas were not as well polished as others; effort was made, however, to achieve a good polish in the center of the flange, where the microscopic analysis was concentrated. Even with careful polishing, some 1-10 μm size features were still evident due to voids or defects in the material, polishing defects, inclusions, etc. For this reason, careful pre-examination was performed by SEM so that any features identified after the irradiation could be verified not to be a pre-existing condition. In order to balance between resolution and areal coverage, a magnification of 105x was chosen for the pre-inspection imaging. With the digital capture resolution available on our SEM, this magnification allowed for the clear identification of surface features larger than 5 μm in diameter. One hundred images were obtained of each flange, moving out 25 mm in four directions from a scribed X in the center of the flange. The total area covered in the pre-inspection consisted of two perpendicular bands 1 mm wide and 50 mm long, centered on each flange.

Fig. 6 shows part of the area of heavy damage on the rear flange of LE3, previously shown in Fig. 4. The arrow identifies the same recognizable grain on the before and after images. Pits in this area were up to 200 μm in diameter. Laser profilometry showed some of these pits to be up to 100 μm deep. Pits typically appeared as roughly hemispherical depressions in the surface, with or without craters due to dislodged material. Fig. 7 shows a cluster of large pits in the heavily damaged region on the front flange of LE3, previously shown in Fig. 3. Shadowing of the electrons collected by the secondary electron detector, which sits at about a 45-degree angle to the surface, produces the light/dark shading that makes the pit topography obvious. The dark spots are relatively deep, sharp walled craters out of which few, if any, secondary electrons reach the detector. Fig. 8 shows some of the pits at higher magnification. The parallel striations within

each single crystal grain are “slip plane” ridges formed by adjacent planes of atoms sliding over one another through the movement of dislocations, evidence that mechanical deformation had occurred. Fig. 9 shows another such pit with an irregular crater at the bottom of the depression.

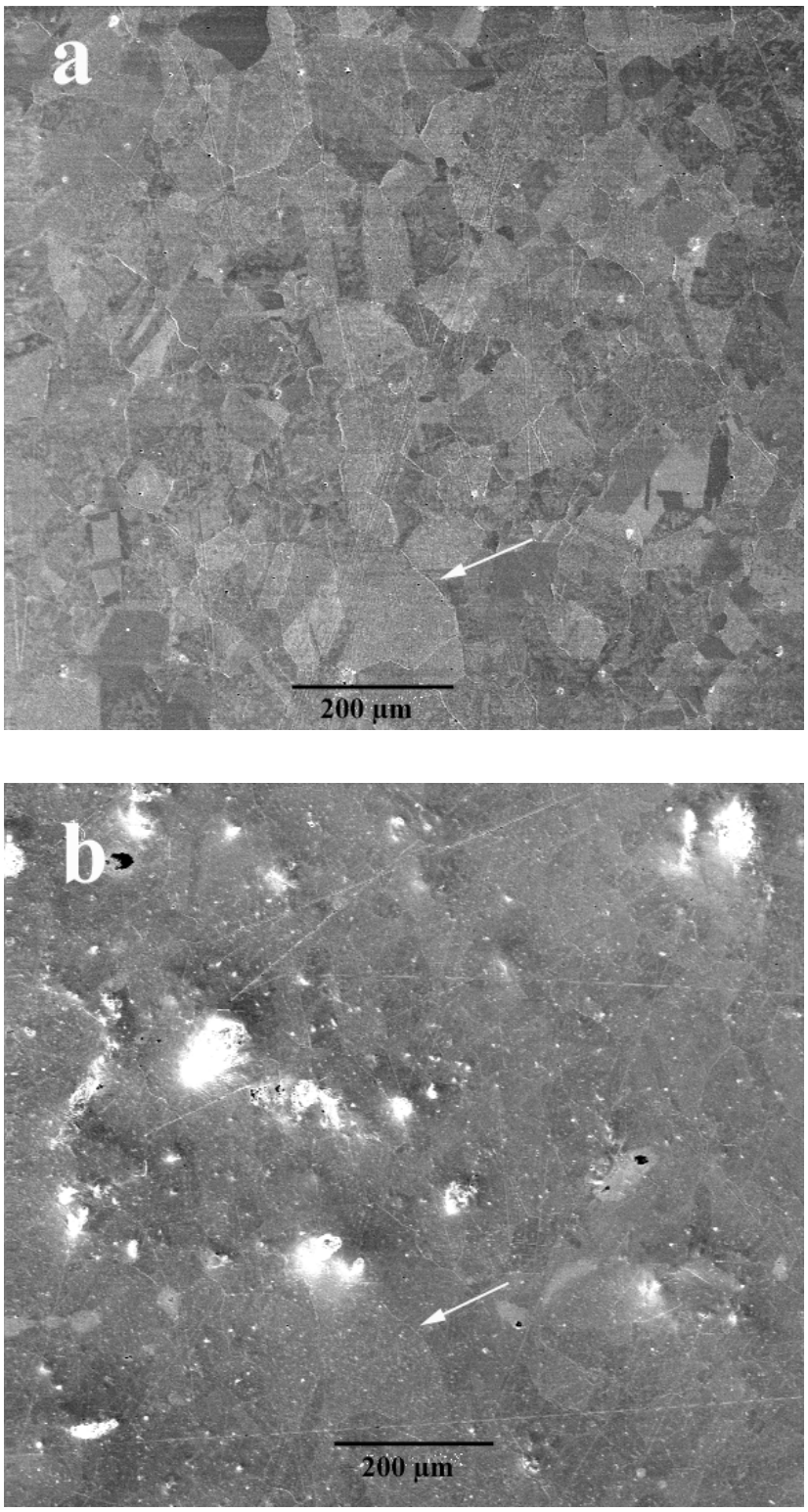

Fig. 6. LE3 rear flange, heavily damaged region (a) before and (b) after irradiation. Arrow identifies the same grain in each image.

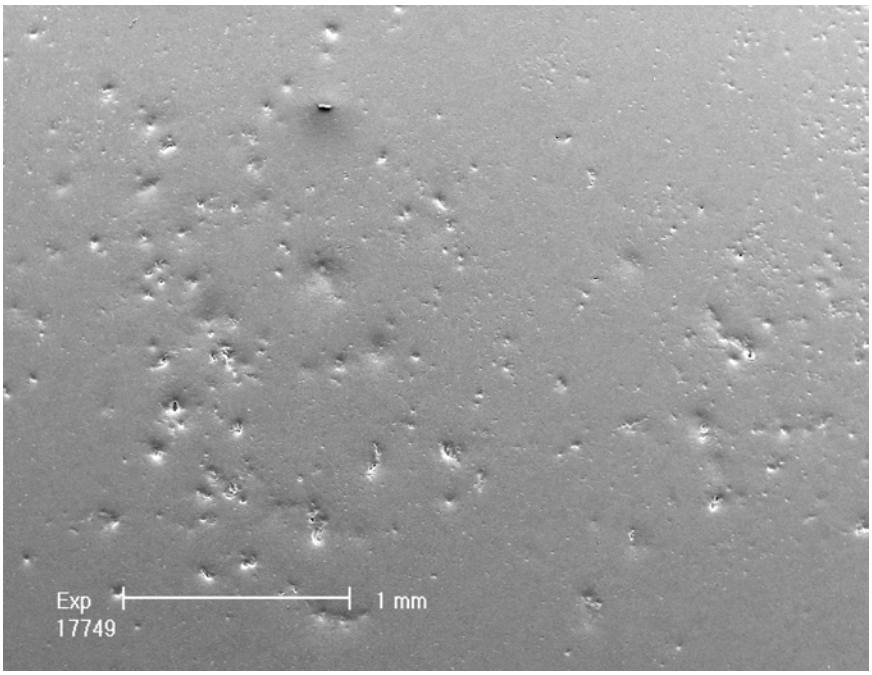

Fig. 7. LE3 front flange, heavily damaged region.

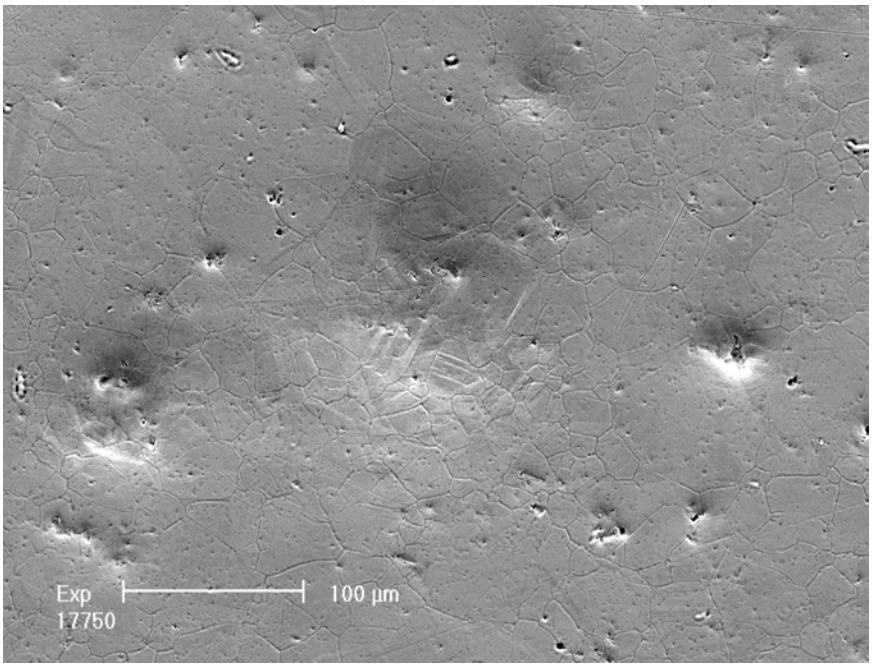

Fig. 8. LE3 front flange, heavily damaged region, slip lines in a large depression.

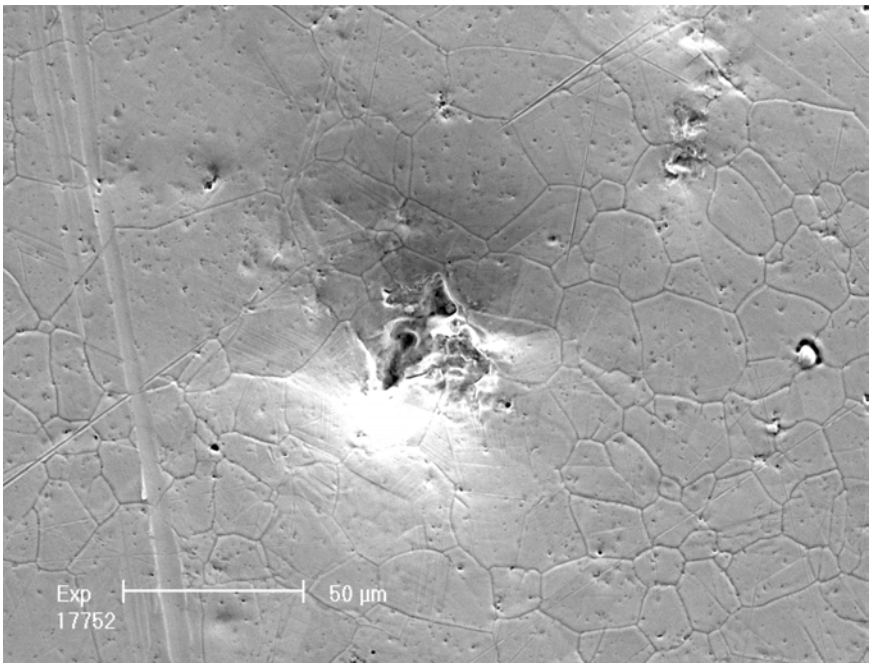

Fig. 9. LE3 front flange, heavily damaged region, crater at the bottom of a pit.

Fig. 10 shows the heavily damaged area from the two rear flanges. The flange from LE4 was not as heavily damaged as its counterpart due to a Kolsterising surface treatment that essentially increases the surface hardness by about a factor of 10. Qualitatively, the pits were the same on the Kolsterised flange, but they appeared smaller and at a lower density. Fig. 11 shows a crater at the bottom of a pit in the Kolsterised flange. Craters like these tended to show strata on the sidewalls. This can also be seen in Fig. 12, which looks down into a large crater in the front flange of LE4.

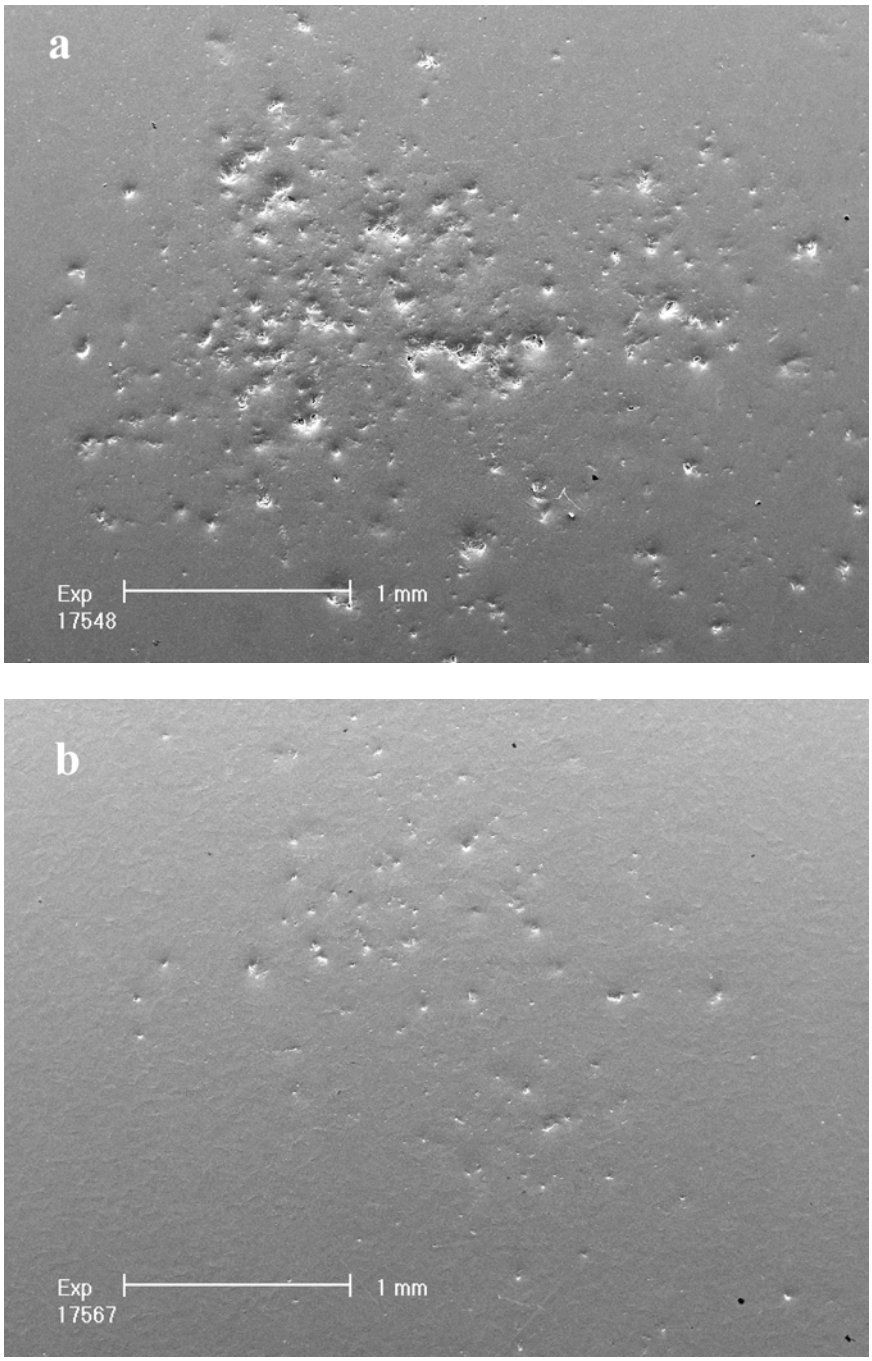

Fig. 10. (a) LE3 rear flange and (b) LE4 rear Kolsterised flange, heavily damaged region.

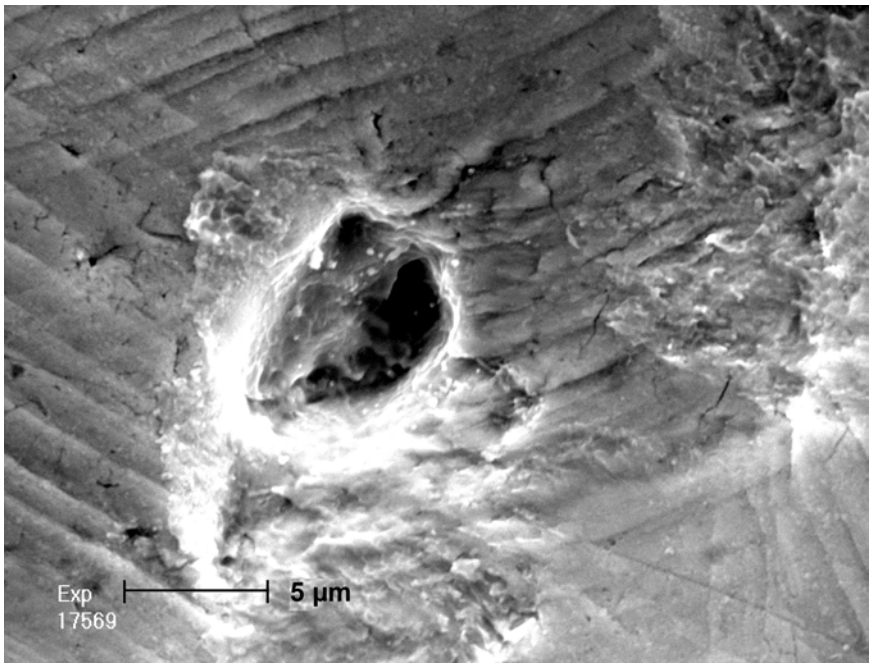

Fig. 11. LE4 rear Kolsterised flange, heavily damaged region, crater.

In addition to the large pits that were obvious upon initial inspection with the naked eye, other smaller 5-20 µm pits were found scattered over the entire surface of the flanges. Fig. 13 shows the center of the front flange from LE3. The surface is pockmarked with small pits that were not there before irradiation. Sometimes these small pits appeared in high-density clusters as in Fig. 14, which shows an area immediately to the right of Fig. 13. The small pits were qualitatively the same as the large pits observed in the heavily damaged region. Fig. 15 shows a crater at the bottom of a small, isolated pit on the front flange of LE4.

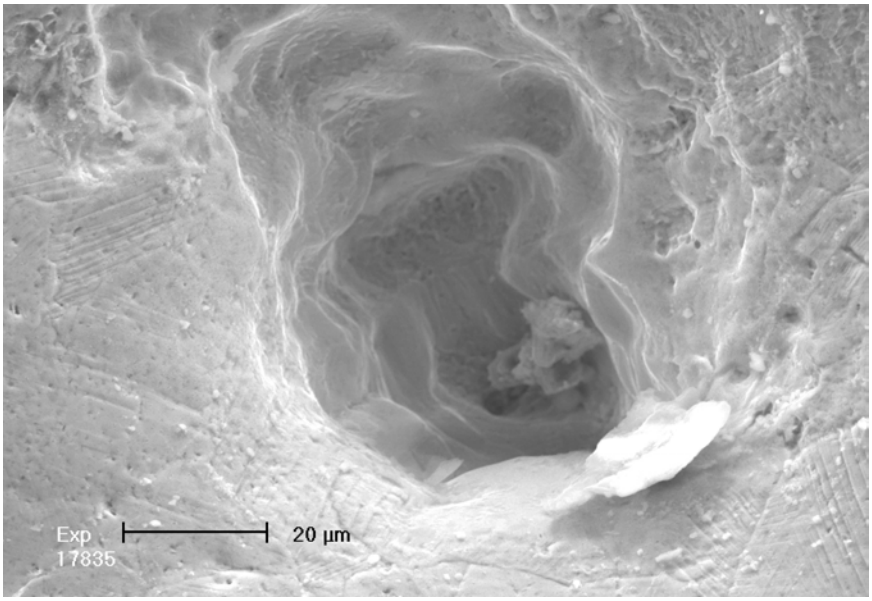

Fig. 12. LE4 front flange, heavily damaged region, crater.

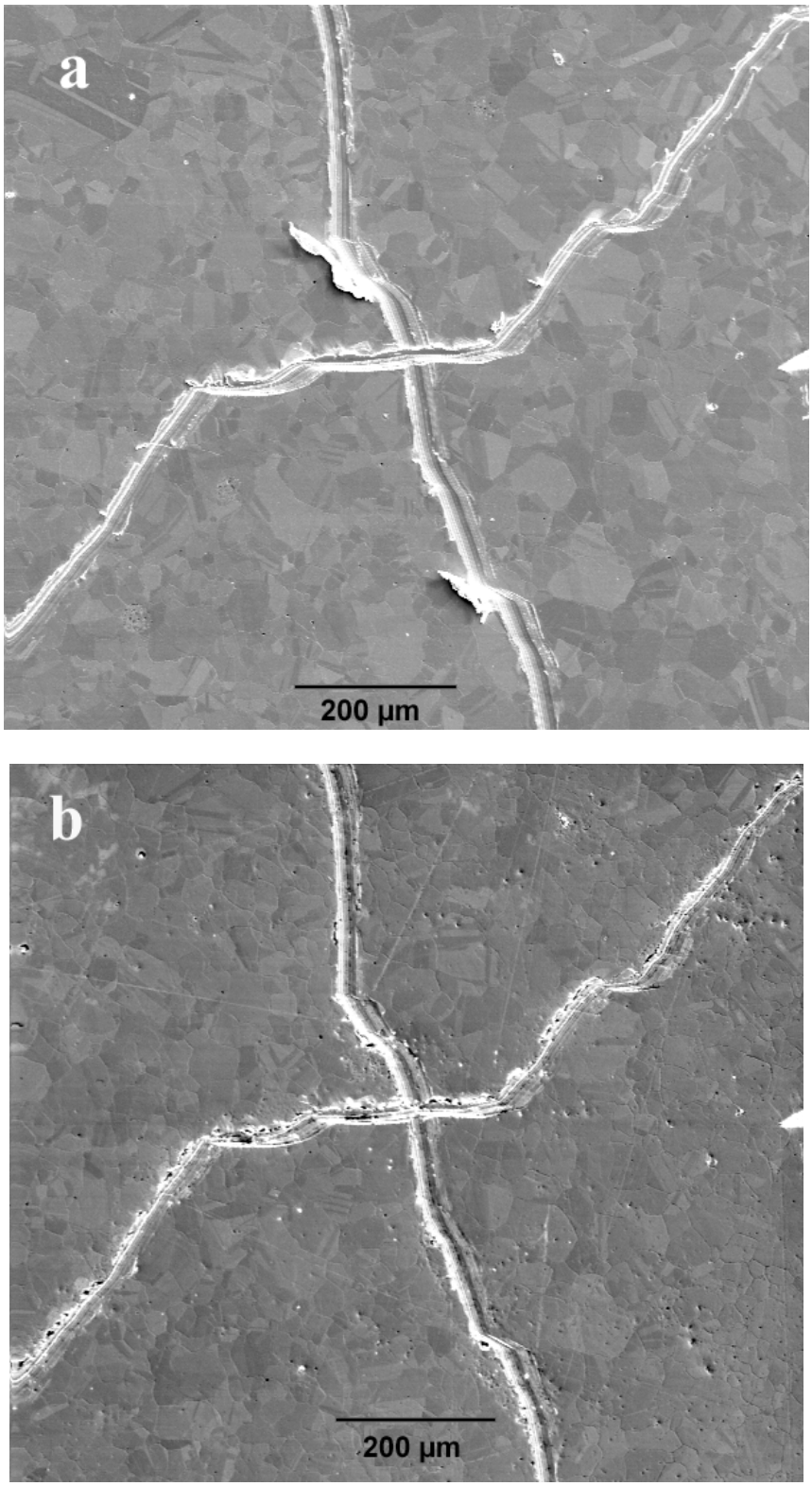

Fig. 13. Center of LE3 front flange, (a) before and (b) after irradiation.

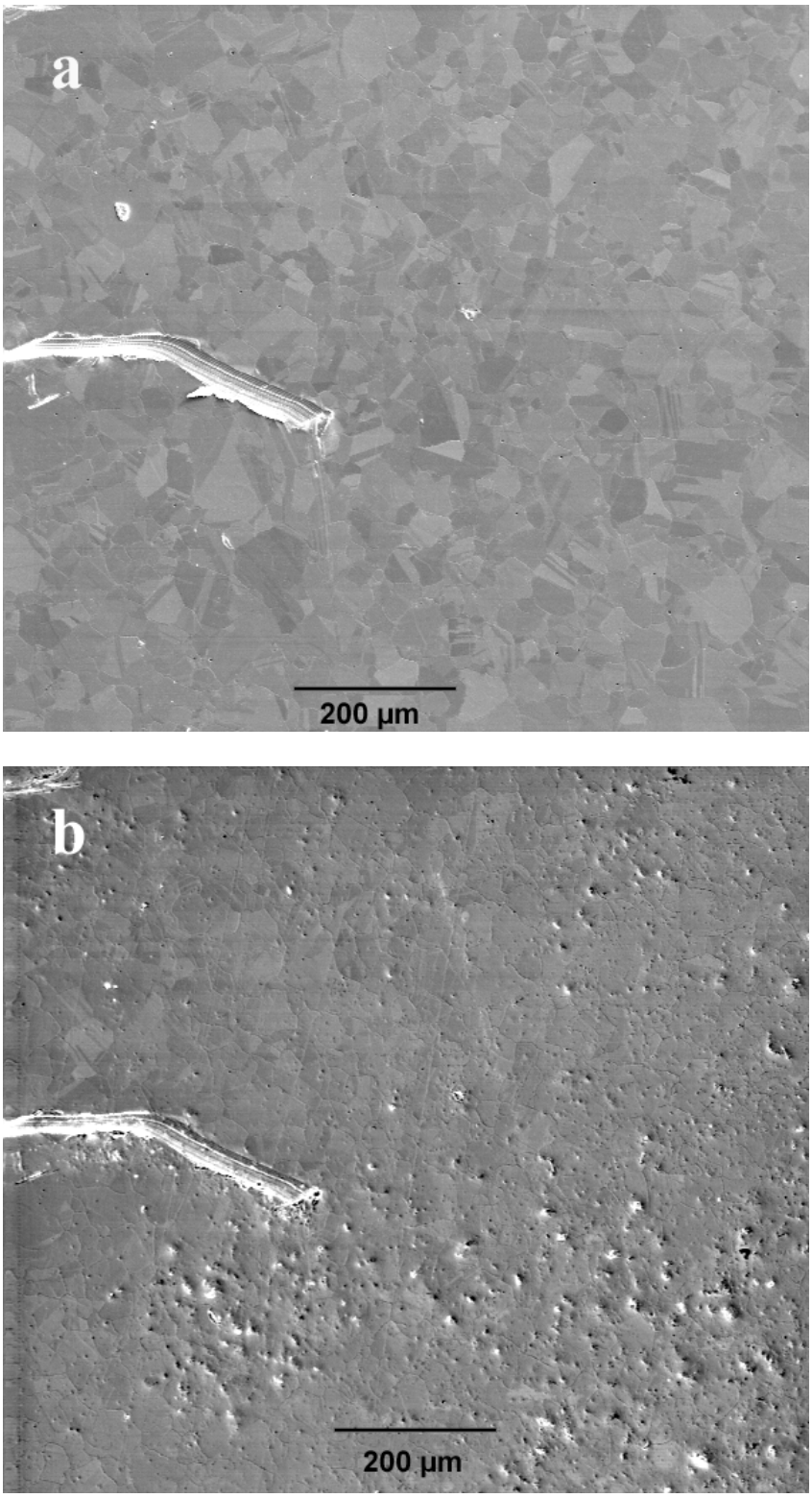

Fig. 14. Just off center of LE3 front flange, (a) before and (b) after irradiation.

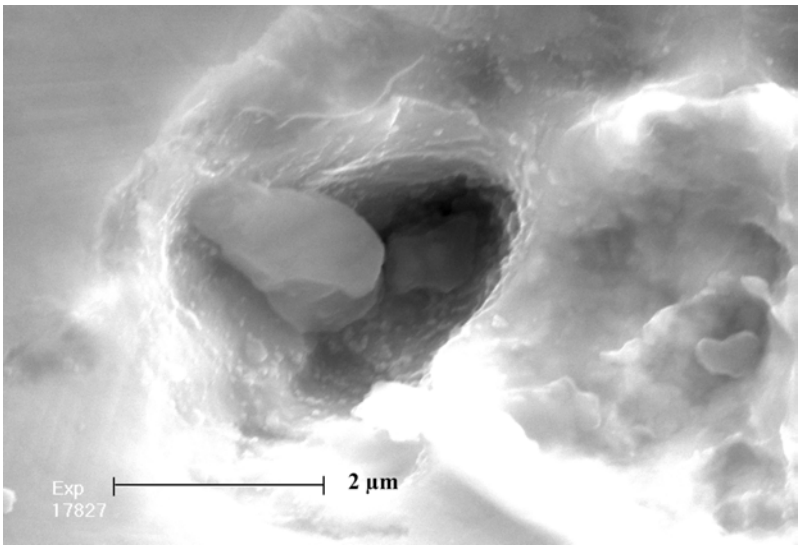

Fig. 15. LE4 front flange, crater in small isolated pit.

Small pits were not as obvious on the Kolsterised surface because there were more than a factor of ten fewer of them (none in clusters), and partly due to the fact that the Kolsterising treatment roughened the polished surface making inspection more difficult. Fig. 16 shows a small, isolated pit on the Kolsterised flange.

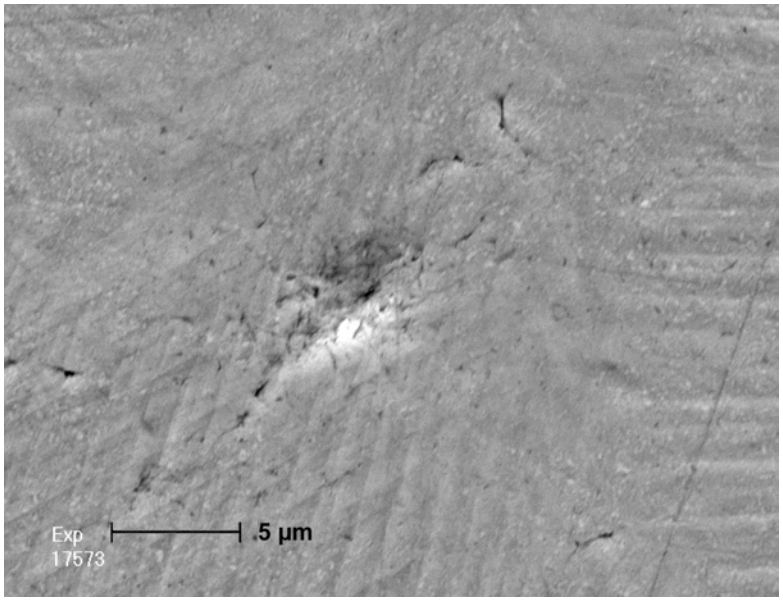

Fig. 16. LE4 rear Kolsterised flange, small isolated pit.

3.1.4 Limitations/shortcomings of WNR tests

- The total number of pulses on WNR test targets has been limited to 200. This is six orders of magnitude lower than the recommended SNS dpa limited lifetime. Significantly more test pulses are not feasible because of facility constraints and difficulties handling higher activation levels. Extrapolating the test results to the SNS dpa lifetime is highly uncertain.
- WNR test targets incur no significant radiation damage effects compared to SNS.
- The WNR pulse repetition rate is limited to 0.03 Hz (2 per minute) vs. 60 Hz for SNS.
- WNR test targets are closed volumes without mercury flow. Including flow may be possible but at considerable increase in test complexity and cost. WNR target geometries for cavitation tests are not prototypic of SNS.
- Polished surfaces were used, in lieu of prototypical surface finishes, to facilitate pre- and post-test examinations.
- Flat surfaces were used in lieu of prototypical shapes to facilitate inspection.
- WNR beam size and total energy are smaller than SNS.
- Each test campaign requires approximately 6 months and $0.5M to prepare, perform, and evaluate test specimens**.**

3.2 Related tests

3.2.1 Mercury Cavitation Threshold Tests

During exposure to short proton beam pulses, mercury will undergo a rapid pressure increase. As the mercury expands, the compression wave eventually reflects as a rarefaction wave from the interface between the walls of its container and the surrounding gas environment (air in our experiments or He in SNS). If low enough pressures are reached in this process, the liquid mercury can break apart (i.e., form cavitation bubbles). It is well known that cavitation bubble collapse can eventually cause severe damage to surfaces. Therefore, it was important to establish whether mercury would cavitate at the pressure levels anticipated for the SNS target, that is, approximately ± 40 MPa. It was also hoped that the presence of cavitation bubbles might act as scattering centers or increase the compressibility of the liquid and bubble mixture, thereby helping to mitigate the stresses in the container wall, but as discussed in the section on WNR testing, no such reduction has been measured. **The tests described below established that**

cavitation is very likely, if not certain, to occur early in the rarefaction portion of the process following exposure of a mercury target to an intense proton beam.

Previous research has shown that for extremely high purity, and degassed mercury, the cavitation threshold is a tensile pressure of several hundred atmospheres, but is much lower for mercury that is exposed to gasses and/or has even extremely small amounts of impurities. To study this phenomenon under more realistic conditions, two types of cavitation threshold experiments were conducted. The first experiments were conducted with an apparatus that measured the cavitation threshold under steady conditions, while the second established the threshold for pressures applied in a transient fashion (25 kHz).

The steady state cavitation experiments used a simple spinner apparatus, shown schematically in Fig. 17, that exerted a tensile load on the central region of mercury filled glass tube rotating at high-speed [1] and [2]. By slowly increasing the rotational speed, the value at which the mercury separates can be determined. As shown in Fig. 18, resulting thresholds range from tensile pressures of about 0.2 to 0.5 MPa, depending to some degree on surface treatment. The threshold was relatively insensitive to temperature for the range examined in these tests (up to 250 ºC). It is believed that cavitation at such small tensile pressure levels was gaseous type cavitation, which resulted from release of previously dissolved gasses, as opposed to vaporization of mercury itself.

The transient tests were conducted in a glass sphere with pressures applied through a piezoelectric transducer at the resonant frequency for the chamber of about 25 kHz (Ref. 2). The cavitation threshold was established based on the onset of large, high frequency fluctuations in the pressure signal measured with a piezoelectric disk microphone that was attached to the outside of the sphere. Results of these tests are shown in Fig. 19 for helium or air cover gas pressures up to 0.3 MPa. Treated surface implies that the glass sphere was heated prior to the tests to drive off as much of the interfacial gases as possible. Cavitation occurred in these transient tests at pressures that were about 0.15 to 0.2 MPa below the cover gas pressure. Surface treatment appears to have only a minor impact.

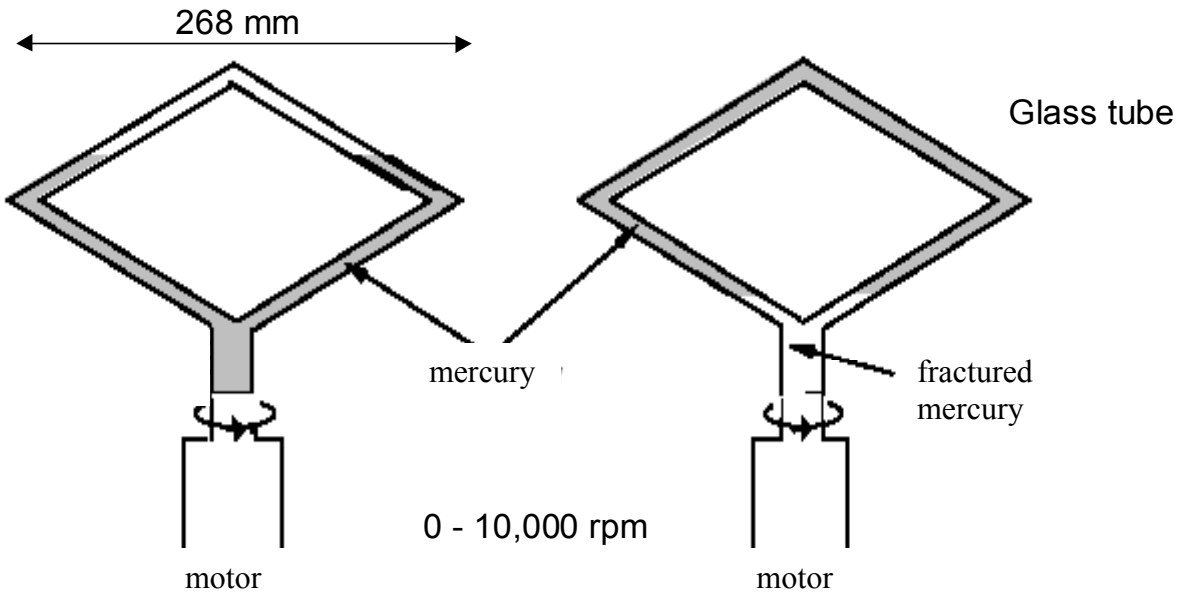

Fig. 17. Schematic of apparatus used to measure the static threshold for mercury cavitation.

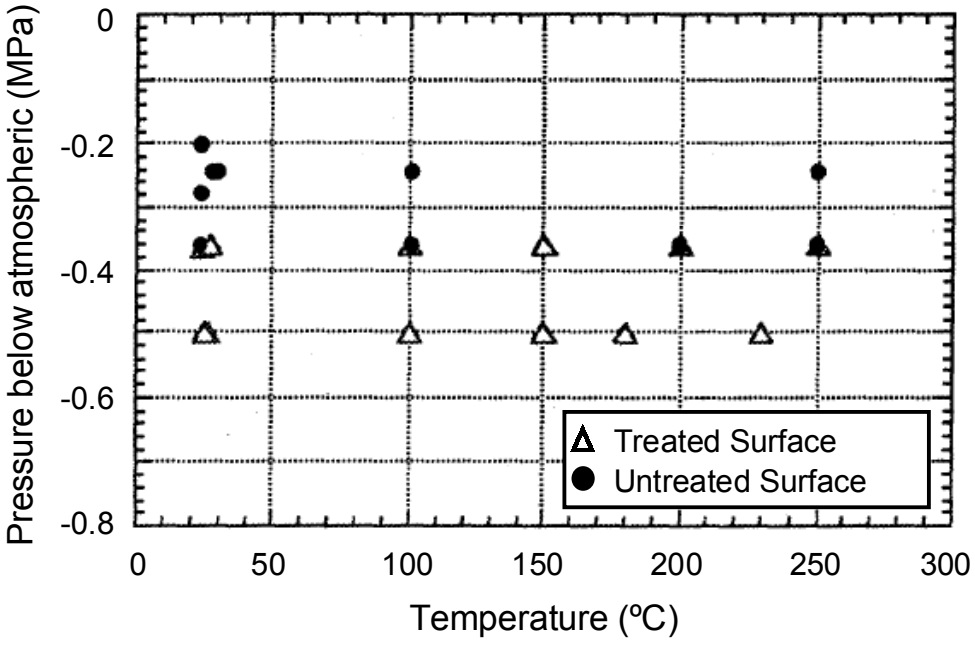

Fig. 18. Static cavitation threshold for mercury.

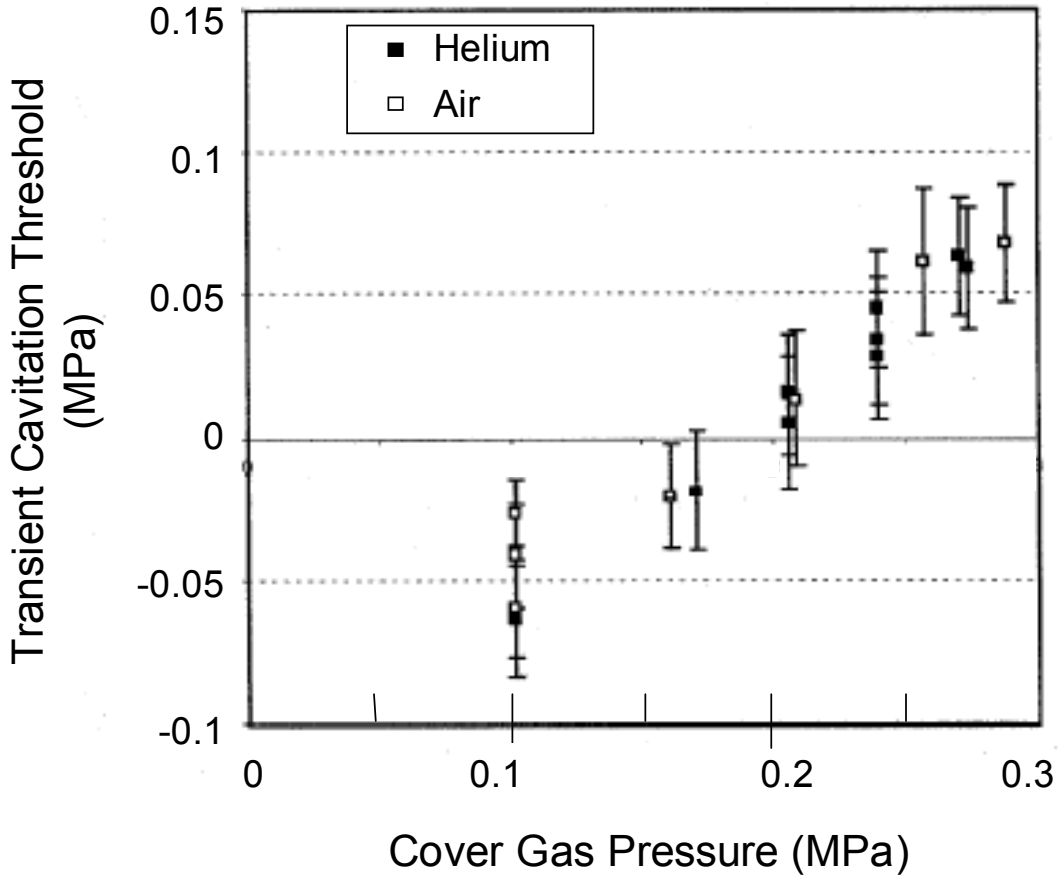

Fig. 19. Cavitation threshold for 25 kHz pressure fluctuation.

3.2.2 Split-Hopkinson Pressure Bar (SPHB)

At the 2nd International Workshop on Mercury Target and Cold Moderator Engineering, held in Tokai, Japan in November 2000, JAERI/KEK researchers presented their discovery of cavitation pitting damage inside the test cavity of their Split Hopkinson Pressure Bar apparatus (SHPB). This mechanical device is normally used to determine material properties under impact conditions; the JAERI team had adapted it for measuring the wave speed of mercury. The impact pressures reached in the test cavity during test were comparable to those created with each proton pulse in the SNS target. This discovery was the motivation for conducting cavitation damage tests for a mercury spallation target.

The JAERI team has conducted a number of tests with the SHPB to investigate cavitation damage. Tested materials included A6061-T6 aluminum (129 Hv), SS316L (not annealed, 211 Hv), Inconel 600 (215 Hv) and Maraging steel (310 Hv). Two impact levels have been used corresponding to cavity pressures of 40 and 80 MPa. Key findings from the SHPB tests are:

- Pits are created with only one impact on SS316L for either pressure.
- The number of pits increases (or eroded area increases) with increasing impacts.
- The number of pits increases with higher impact pressure.
- The maximum number of impacts on a set of cavity specimens has been 100.
- The degree of damage of the materials ranks inversely with the material hardness: A6061 > SS316L >Inconel > Maraging steel.

The JAERI team also tested SS316 (not annealed) with Kolsterising surface treatment, at the request of SNS Target Systems. Their test was limited to the case of 80 MPa and 10 impacts, but the result was no clearly observable pits. The same difficulty of inspecting a rough surface was encountered as with the Kolsterised WNR target flange.

Limitation of SHPB tests

- The SHPB test applies pressure to the mercury through a solid material interface. This is in contrast to a spallation target where pressure is generated internally in the mercury via volumetric energy deposition.
- The SHPB test cycle takes considerable time due to alignment checks and other preparations needed for every impact. The apparatus cannot practically be used for more than a few hundred pulses per test specimen, i.e., the number of impacts prototypic of the SNS target are not possible.
- The SHPB is a JAERI apparatus. There are limits to the resources they can provide for future testing for our benefit.
- Only small, flat, and highly polished specimens can be used.

3.2.3 Liquid metal target experience at CERN

The CERN–ISOLDE facility produces radioactive ion beams with liquid metal targets. The facility can produce pulses with 3×10^{13} protons within 2.4 microseconds. Their initial report of shock type damage is given below for tantalum targets with molten lead:

ISOLDE NEWSLETTER

July 1994

"In the last tests of the molten metal targets the splashing from the surface the metal following the shock wave induced by the proton beam pulse could efficiently be damped and kept out of the ion source by means of a chimney equipped with baffles. This allowed to operate the targets somewhat longer. Unfortunately this only lead to the discovery of a new deleterious effect of the shock wave, which causes the targets to fail. In fact a cavitation like effect which both corrodes and stresses the beam entrance wall of the target container and causes welds to break so that the charge of molten metal is lost through leaks. During the shut down autopsies in the hot cell on a number of failed targets allowed us to document the damage caused by this effect. …."

The following was documented in 1995 in a paper presented at ICANS XIII:

Target designs were improved by increasing the wall thickness, changing the weld design from TIG to e-beam with the weld located away from the beam and protecting the window with a pyrocarbon disk.

Recently tests have been conducted at CERN and at Brookhaven National Laboratory with mercury in pulsed proton beams, in support of the Muon Collider and Neutrino Factory design development. Tests with mercury in a cup with a free surface confirm high initial pressures by measurement of high surface velocities on the order of 10's of meters per second.

4.0 Comparison of strain predictions with measurements

This topic is not directly related to the cavitation damage issue, but it is an outstanding problem for the mercury target design. An incomplete physical understanding of the cavitation process during a beam pulse has made structural modeling of the mercury – vessel system, including pressure wave propagation with cavitation effects, a difficult analysis to perform. A hoped for empirical model based on experimental results has not been obtained.

Efforts to simulate the mechanical response of mercury target vessels have been underway for several years. Pressure waves induced by the rapidly deposited energy from each proton pulse propagate through the mercury and interact with the vessel leading to a complex dynamic stress response. The simulations would provide the basis for estimating the fatigue life of the SNS target vessel. While early attempts using simplified target geometry suggested the approach could estimate these dynamic stresses, it was clear that experimental results were vital to calibrate the simulations and gain confidence in the approach The first credible strain measurements made on mercury targets with beam intensities similar to the SNS were performed in August 2000 tests at the WNR facility [3].

Confidence in the simulation approach has not been achieved. Although the predicted response of a graphite target shows excellent agreement with measurements, attempts at simulating mercury test target response have yet to provide a good match to measured strains. The main difficulties are the lack of adequate descriptions of mercury's behavior (bulk modulus, or wave speed) over the expected range of pressures (positive and negative), and of the interaction between the mercury and vessel (i.e., the contact behavior).

Using the nominal wave speed of mercury (about 1460 m/s) in simulations with interface behavior that supports both tension and compression typically gives strain response frequencies that are higher than those measured in experiments. Sometimes the earliest part of a response is reasonably predicted, but soon after, measured strains reveal lower frequency and sometimes larger magnitude response than those predicted.

Some examples of simulation and measured strain data follow from WNR tests on "Large Effects" targets. Fig. 20 and Fig. 21 show strains at sensor locations on the thinned portions of the front and rear flanges. Predicted strain is shown for two cases: (1) nominal mercury wave speed and contact behavior; (2) mercury wave speed reduced to 20% of nominal, softened tensile contact behavior, and applied beam energy scaled by the reduction of wave speed (scaling

chosen to give improved match in predicted strain magnitude). Measured strains from three WNR tests shown in Fig. 20 and Fig. 21 include two from LE1 (tested August 2000) with mercury de-gassed in one case and with a modest overpressure of helium in the other. The LE4 strains (July 2001) also used helium, but had fully annealed flanges.

The nominal simulation significantly under predicts the measured strains at both front and rear locations. During the first 0.5 ms, the prediction roughly follows measured values for the rear flange. Afterwards the actual rear strains grow considerably and oscillate from negative to positive. The reduced wave speed simulation case does a somewhat better job of matching the compressive strain magnitude and oscillation at a low frequency, but it does not predict the large tensile values measured. The reduced wave speed simulation is also better than nominal at the front location. The simulations are not adequate at either location.

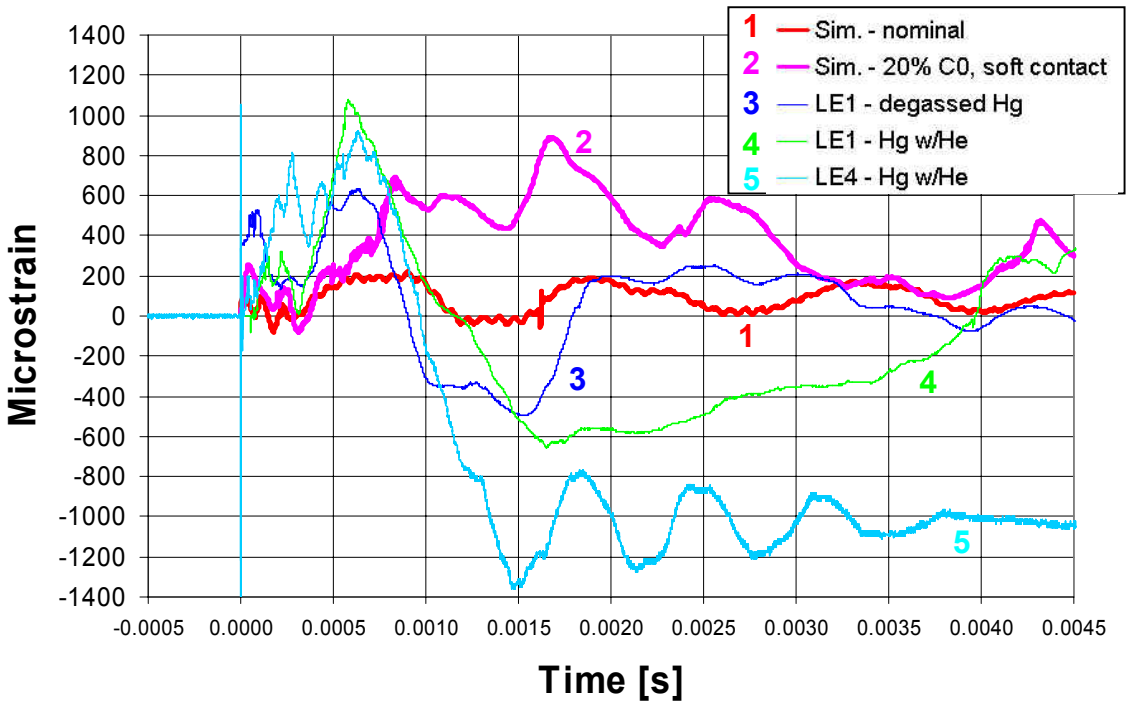

Fig. 20. Simulated and measured data from LE target, front center.

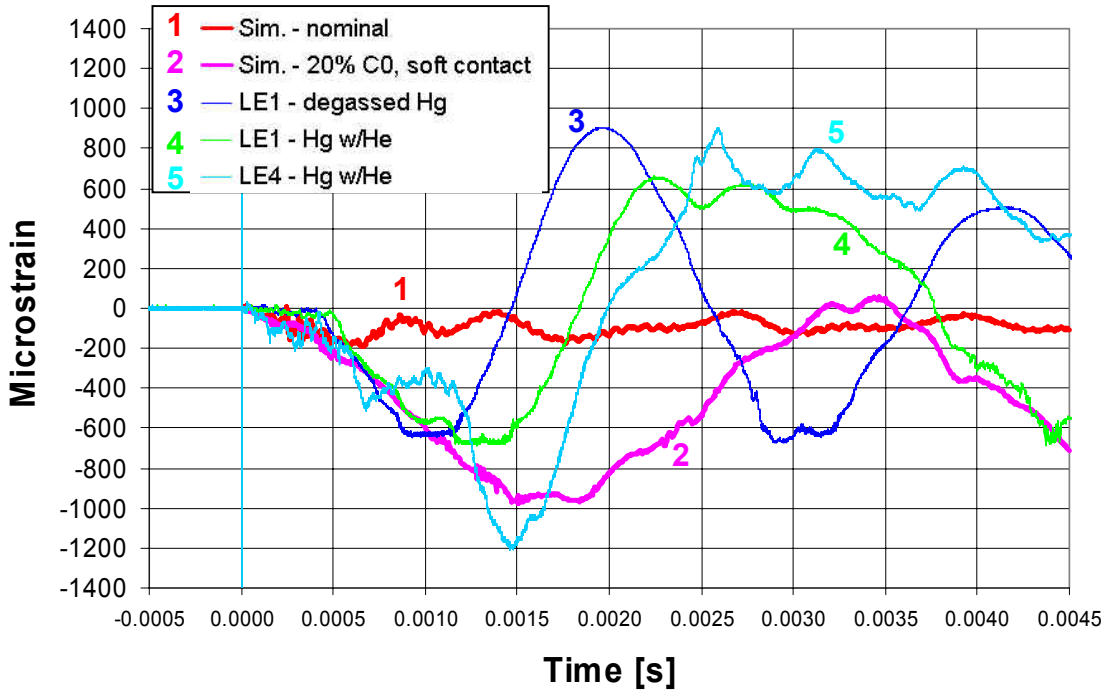

Fig. 21. Simulated and measured data from LE target, rear edge.

Review of mercury pressure evolution from either simulation predicts that very large fluid tensions are produced at various times, on the order of hundreds of atmospheres. Based on bench top experiments, gaseous cavitation is expected at only a few atmospheres tensile pressure. The presence of gas bubbles formed by cavitation will greatly change the effective wave speed in the mercury. No means to predict the spectrum of bubble sizes, their volume fraction, or their lifetime has been found. Wave speed in a bubbly mixture is highly sensitive to these parameters [4].

For any given target and test condition, the experimental data has been repeatable, giving hope that an empirical description of the behavior of mercury could be found. Regretfully this has not yet happened. The current situation is that there is no means to confidently predict the fatigue life of the target.

Strain predictions made for the ASTE target have shown excellent agreement with experimental measurements, however considering this target's geometry and the nature of the energy deposited by the AGS proton beam, the interaction between the mercury and target vessel is weak. The stress wave propagated primarily through the vessel itself. This is not characteristic of the SNS target.

5.0 Hypotheses on pitting mechanisms

Although there have been no direct observations of the mechanism responsible for the pits found in post-test inspections, three mechanisms or factors that might have caused or at least contributed to the damage have been seriously considered. These mechanisms are:

(1) Cavitation bubble collapse,

(2) Radial focusing of pressure waves in an axisymmetric target, and

(3) Large mechanical strains, well into the plastic range.

These three mechanisms are not mutually exclusive, i.e., two or possibly all three mechanisms could have worked together to cause the damage observed in the July 2001 mercury target tests at the WNR facility. Item (1) is probably happening; the other two may be making it worse. Each of these three mechanisms is briefly explained below. It should be noted that the combination of mechanisms (2) and (3) above was specifically addressed in the December 2001 tests where thick diaphragms, yielding low strain, were used on a non-axisymmetric (rectangular cross section) target.

Current understanding of cavitation damage mechanisms are summarized in the next section of this report; however, it should be noted that the pitting damage we see in the micrographs of diaphragms irradiated at the WNR facility are typical of the type observed in cavitation bubble collapse. Given this observation along with the indications from our theoretical predictions that we easily achieve tensile pressures that reach the threshold we have measured for cavitation, it seems highly probable that the pits are caused, at least in part, by cavitation bubble collapse.

Radial focusing of the pressure waves in the axisymmetric targets used in the July 2001 tests is the most likely explanation for the location of the large pits. A photograph of the mercury-facing surface of one of the end-plate diaphragms from these tests is shown in Fig. 5. As shown in the photo, large pits, visible to the naked eye, are distributed over a region that is about 5 mm in diameter and centered about 10 mm directly below the center of the diaphragm. Using activation analysis techniques, the beam was found to be centered approximately 5 mm directly above the center of the diaphragm. This 180º shift between the beam center and center of the region with large pits is thought to be due to radial focusing of the pressure wave and its reflection off the side walls of the cylinder. The question remains whether these pits are caused by the collapse of the rarefaction wave as it reflects from the side walls of the cylinder, resulting in intense cavitation near the center of the diaphragm, or are they the result of impingement of an

axial jet of mercury on the diaphragm due to radial focusing of compression waves, or some other mechanism. Although it is unlikely that the December 2001 tests may resolve which of these hypotheses is correct, the question of whether radial focusing is a primary factor in generating the large pits should be answered after inspecting the diaphragms from the rectangular cross-section target.

The very large strains and deflections developed in the central region of the thin windows used in the July 2001 WNR tests may have also contributed to the number and size of the more or less centrally located “large” pits. A typical strain measurement for a sensor located near the center of one of the diaphragms is shown in Fig. 22. The elastic limit for the strain of the annealed 316SS is expected to be about 850 micro-strain. Clearly, this diaphragm underwent plastic deformation. Although it is highly unlikely that this strain by itself caused the pitting, there is some reasonable probability that this was a contributing factor. Furthermore, the reaction of this central region of the window to the initial pressure pulse causes a large, rapid movement of this region, which may lead to separation of the window from the mercury (cavitation). One argument against these mechanisms is that the large pits were not exactly in the center of the diaphragm or the center of the beam (see Fig. 5 * MERGEFORMAT and the discussion in the previous paragraph). Whether or not this is an important part of the damage story should be answered soon, since five of the six mercury targets tested in December 2001 at the WNR facility used much thicker diaphragms that had much lower strains.

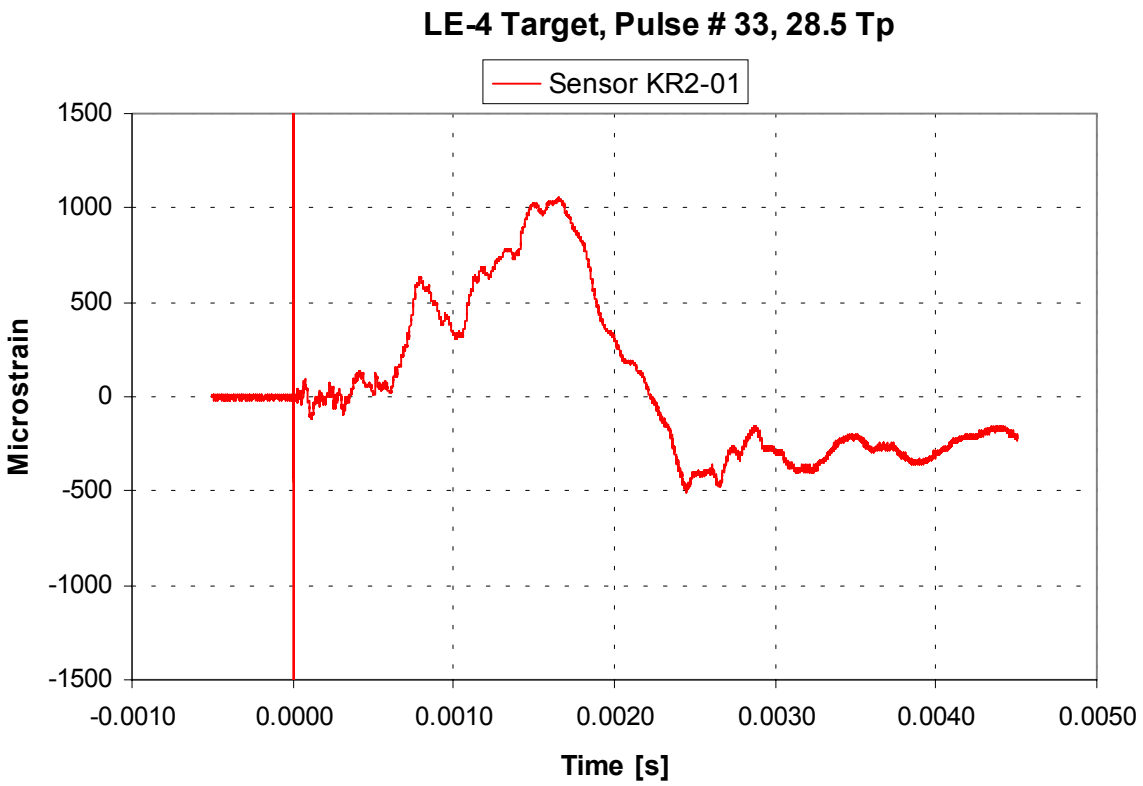

Fig. 22. Typical strain response for a region near the center of an LE target diaphragm following a proton beam pulse from July 2001 WNR tests. Since the elastic limit is approximately 850 micro-strain, this region underwent significant plastic deformation.

6.0 Impact on Hg Target Design and Lifetime

6.1 Present design basis

The current mercury target vessel design is a result of a five-year optimization process involving a complex set of design requirements and parameters including:

- Neutronic performance
- Material selection
- Structural integrity
- Thermalhydraulic performance
- Spent target handling and disposal
- Affordable costs

Austenitic stainless steel type 316 (grade L / LN) was chosen as the material for the mercury target vessel based on:

- Its chemical and metallurgical compatibility with mercury over an acceptable range of temperatures, and
- The availability of a large database of acceptable structural properties for both the normal and irradiated conditions, supplemented by data on fatigue allowables in mercury from the SNS R&D program.

The derived target design, and cost estimate, is based on available 316 L(N) stock sizes, manufacturing techniques, and welding and weld inspection technology. The target life is limited by changes in material properties due to irradiation, and the remote maintenance and spent target handling techniques being planned are based on after heat and material activation levels applicable to 316.

Extensive, though incomplete, static and dynamic stress analysis has been conducted on the target vessel. Especially critical is the sizing of the proton beam windows and their attachment to the target body. The inner window thickness of 0.050 inches (1.3 mm) is thick enough to withstand the static pressure of the circulating mercury and pressure waves from thermal shock while being sufficiently thin to limit the temperature rise and thermal stress arising from proton beam energy deposition. The 0.13 inch (3.3 mm) gap between the two beam windows is sized to provide mercury flow velocity sufficient to cool the windows. The outer window's thickness is also 0.050 inch (1.3 mm), for reasons similar to the inner window. The curvature of the windows

not only determines the mercury flow pattern but is also important in establishing the level of stress in both the window and the weld attaching it to the main target vessel body.

6.2 Effects of pitting on the target vessel structure

While it is obvious that an accumulation of clusters of large pits seen on the WNR test targets would result in failure of the target vessel's mercury pressure boundary, there are also concerns arising from the presence of the smaller, more distributed pits seen on the test samples. The principal issues are:

- The manner, in which these pits accumulate over the life of the target, could erode the surfaces sufficiently to fail the pressure boundary.
- The effect of the resulting material surface condition, possibly in combination with a reduced effective material thickness, on the fatigue life of the target beam windows is unknown. Furthermore, there is no practical method to produce fatigue test samples with the corresponding surface condition.
- There is a limited ability to predict the areas subject to damage, resulting in a concern about the effects of accumulated damage on components expected to last the lifetime of the SNS facility.

The uncertainty of the testing and results place an increased importance on obtaining additional data during early SNS operation. To do this a method must be developed to perform post-irradiation inspection of spent targets.

If, in the worst case, the pitting results in unacceptable life times for mercury targets, a very difficult, costly, and time consuming effort will be required to remove the mercury cooling loop, decontaminate the hot cell, dispose of mixed wastes, and install a water cooling loop.

6.3 Issues with options for eliminating pitting

There are several techniques currently being considered for eliminating, or at least controlling the amount of, pitting on the target vessel. In general, these involve a change of the target vessel material, adding a cavitation resistant coating to the base material, and/or changing the target geometry. Design issues related to these solutions are outlined below.

- Issues with changing materials
  - No or limited data base on irradiated mechanical properties
  - Material availability, manufacturability limitations, cost
  - Spent target after heat, radiation levels, handling
  - Joining of the new material to balance of system - location of transition
  - Properties of weld material and heat affected zone
  - Unknown compatibility with mercury
- Issues with coatings
  - How & where they can be applied, control of quality
  - Effect of process temperatures on base material properties
  - Coverage of weld joints
  - Required thickness - life
  - Unknown compatibility with mercury
  - Unknown irradiation properties
- Issues with changing target geometry
  - Limits on space and shape of target zone in reflectors, moderators, inner plug, etc
  - Changing of the flow pattern
  - Cooling of window
  - Recirculation zone on baffles

7.0 Review of cavitation damage literature

7.1 Definitions

The term ‘cavitation erosion’ refers to loss of material from a solid surface by exposure to a cavitating liquid. The liquid can be stationary or flowing. Cavitation erosion is not a corrosion phenomenon. It is mechanical damage. If cavitation erosion and chemical corrosion occur together, they can be strongly self-reinforcing. The impacts in cavitation erosion are pressure-related and may be initiated by fluctuations in flow or by imposed vibrations. In fluid dynamics, a cavity is a void or bubble in the liquid medium. To avoid confusing this cavity with the cavities or indentations produced at the solid surface, the latter will hereafter be referred to as surface craters or pits. Going further, a pit without a break in its surface will be defined as a dish or depression. A pit from which material has been removed will be called a crater.

7.2 Information sources

The information on cavitation erosion is abundant; most of it devoted to cavitation in water. Our understanding of cavity formation and collapse in liquids begins with the seminal studies of Lord Rayleigh [5] on an imploding spherical cavity. Two good literature reviews of cavitation erosion are by Hammit [6] and Hansson and Hansson [7]. A third review by Karimi and Martin [8] emphasizes the materials aspects. A review of liquid droplet erosion, which is related by similar physical processes to cavitation erosion, is given by Heymann [9]. Two outstanding papers on the basics of damage mechanisms are Tomita and Shima [10] and Philipp and Lauterborn [11]. Two books on cavitation are by Knapp et al [12] and Brennen [13]. The information on cavitation in mercury is sparse. Early papers on the topic are by Garcia et al. [14] and Young and Johnson [15]. More recently, work in connection with liquid metal spallation targets has been carried out by West [16], Kass et al. [17], Pawel et al. [18] and Futakawa et al. [19].

Standardized methods have been devised for conducting cavitation erosion tests. The most common method, particularly for comparative screening of the erosion resistance of different materials, is high frequency sonic vibration [20]. Bar charts of materials rankings compiled from such tests are available in Ref. [6](p. 190). Bar charts of erosion rate rankings for liquid droplet erosion are available in Ref. [9] (p. 229), and are very similar to those for cavitation erosion.

7.3 Summary of information

Cavitation erosion of a solid surface is caused only by those cavities that collapse at, or very close to, the surface. Shock waves and high-speed liquid jets from the collapse strike the surface with sufficient force to deform and gouge it. Many materials, such as metals, rocks, concrete, polymers, etc., have been investigated for cavitation erosion responses in water under many conditions, and it seems that all materials can be made to pit under the right conditions. It is important to note that no exceptions have been reported. From the literature, it is clear that although a great deal is known about the phenomenological aspects of pitting and the basic processes that are in operation, no permanent cure has been found. However, some materials are more resistant to pitting than others, under similar circumstances. Some coatings and surface hardening treatments afford improved resistance but they may be effective, or not, depending on the intended service life compared to the time interval for the erosion of the protective surface region. Materials that undergo progressive work hardening or phase changes as a result of the surface impacts offer more persistent resistance. Cavitation erosion rates in liquid mercury are up to 20 times higher than in water. Pitting mitigation strategies must use a combination of materials improvements and cavitation abatements.

7.3.1 Cavity formation and collapse

Cavities are formed by local fluctuations of pressure in the liquid. Tensile pressures can open cavities in the liquid. Such pressures can be found in turbulent flow regions and in rarefaction pressure waves caused by vibration or impact. If a cavity migrates to a region of higher pressure, or if it encounters a compressive pressure wave, it collapses. The driving forces for the collapse are the difference in pressure between the local hydrostatic pressure and the vapor pressure in the cavity, and the capillary force due to surface tension that increases as the cavity size decreases. Ignoring the increase in collapse velocity from surface tension, the collapse velocity, v, varies as $[(P-P_v)/\rho]^{1/2}$, where P is the hydrostatic pressure, P_v is the vapor pressure, and ρ is the density of the liquid. For a cavity with an original radius of one mm, collapsing under one atmosphere overpressure in water, the collapse velocity is approximately 100 m/s [7]. The collapse time typically is about 10 μs in water. The collapse entails a sudden inflow of liquid, generating a high pressure near the center of collapse and emitting an associated shock wave. Some of the energy of the collapse is dissipated as heat so intense as to emit visible light. Analyses of the light

flashes indicate temperatures of 5,000 – 10,000 K. The duration's of the flashes are only tens of picoseconds. It is not known whether the heat of cavity collapse is involved in pitting.

Collapses in cavities located away from a solid surface occur symmetrically inward and are non-damaging to the surface. Surface erosion is caused by collapse of cavities that are located on the solid surface or very close to it. The presence of the solid boundary induces pressure gradients that distort nearby cavities; collapse is asymmetrical and is directed towards the solid surface. A consequence of this interaction is that fluid flow in the region between the collapsing cavity wall and the boundary is reduced and the pressure becomes higher at the opposite cavity wall, forcing the cavity center towards the boundary. This motion towards the boundary is accelerated in the final stages of collapse and it ensures that all cavities whose centers are within a distance of one cavity diameter from the surface will collapse on the surface.

Another consequence of distorted cavities and their asymmetrical collapse is that the influx of liquid is non-symmetrical. A liquid cone, or jet, is formed that passes through the center of the collapsing cavity immediately before complete closure, thus changing the shape of the cavity from spherical to toroidal. There are two types of impact on the surface, a shock wave from the violent collapse and a liquid hammer from the jet. In detail there are at least two shock waves, one from the compressive collapse and one initiated when the liquid jet descends from the top of the cavity and hits the internal surface of the cavity closest to the boundary [11]. The impacts occur in time scales of microseconds and the impact stresses may have magnitudes as large as 1,000 MPa [8], which exceeds the yield strength of most metallic materials. They plastically deform the solid surface, resulting in dished or cratered pits.

7.3.2 Pit formation and erosion progression

It is well demonstrated that the pits formed in cavitation erosion are developed by local plastic deformation and fracture under the impact forces of cavity collapse. Strain rates are very high, of order 10^4 to 10^6/s. In contrast, a common strain rate for a tensile test is 10^{-3}/s. Thus, all other things being equal, strain rate sensitive materials have been reported to experience worse cavitation erosion than those that have lower strain rate sensitivity. The relative contributions of the jets and the collapse shock waves in the formation of pits are a matter of disagreement in the literature. The relative contributions are found to depend on the original size of the cavity and its location with respect to the boundary at the moment of implosion. The strength of the shock

wave is attenuated in proportion to the inverse of the square of its distance from the collapse center, whereas the jet exerts it largest force at its tip. It is believed that material is lost from the surface by a variety of mechanisms including impact fracture, shearing of protruding crater rims, and fatigue crack propagation.

Pit formation in response to these impacts is generally acknowledged to be a complex process. The shape, depth, and appearance of pits will depend on the nature of the forces acting on the pit region, which depend on the technique used to generate the cavity. Pit formation mechanisms are not well understood. It is assumed that forces dominated by the collapse shock wave should give simple compressive stresses that should favor dishing. Repeated impacts of this type can lead to impact fractures, fatigue crack propagation and loss of material. Forces dominated by the jet will entail a strong shear component that could gouge out material. Tests made with single cavity collapses produced by a vortex cavitation generator or a Francis turbine show pits that are deeply gouged, are irregular in cross section, and have raised rims. Tests in a vibratory device show that the surface first becomes undulated and marked with deformation bands before pits are formed [8]. Of course, brittle materials will crack and chip off under such shock loading. It is known, too, that cavities tend to gather in clusters. The collapse of one cavity can produce pressure transients that may trigger the collapse of nearby cavities. If clusters collapse in concert, the damage will be more concentrated.

It is recognized that chemical corrosion can exacerbate removal of material to form craters. Protective films on the surface tend to be much less ductile than the substrate metal, and under repeated blows they can spall off, exposing the bare substrate to chemical attack. In aqueous media, absorption of hydrogen may cause embrittlement. Even in the absence of chemical dissolution and hydrogen embrittlement, spalling of an oxide film will encourage self-renewal of the film, and the spallation/renewal cycle will accelerate removal of the substrate.

Establishment and measurement of erosion rates requires sampling of many pits in reasonable time periods, and simple techniques for gauging the erosion. The most convenient and rapid method is a standardized procedure of acoustic vibration using coupons of the test material on which erosion is measured by weight loss at intervals [20]. Despite the standardization of this technique, the erosion rate depends very strongly on the particular test conditions, and is not especially reproducible or controllable. In general, though, it follows a nucleation and growth route, whereby there is an incubation phase (in terms of time or number of

impacts), where the erosion rate is small, followed by a rapid growth regime which then settles down to a slower growth phase. A schematic depiction of the stages of erosion progression is shown in Fig. 23.

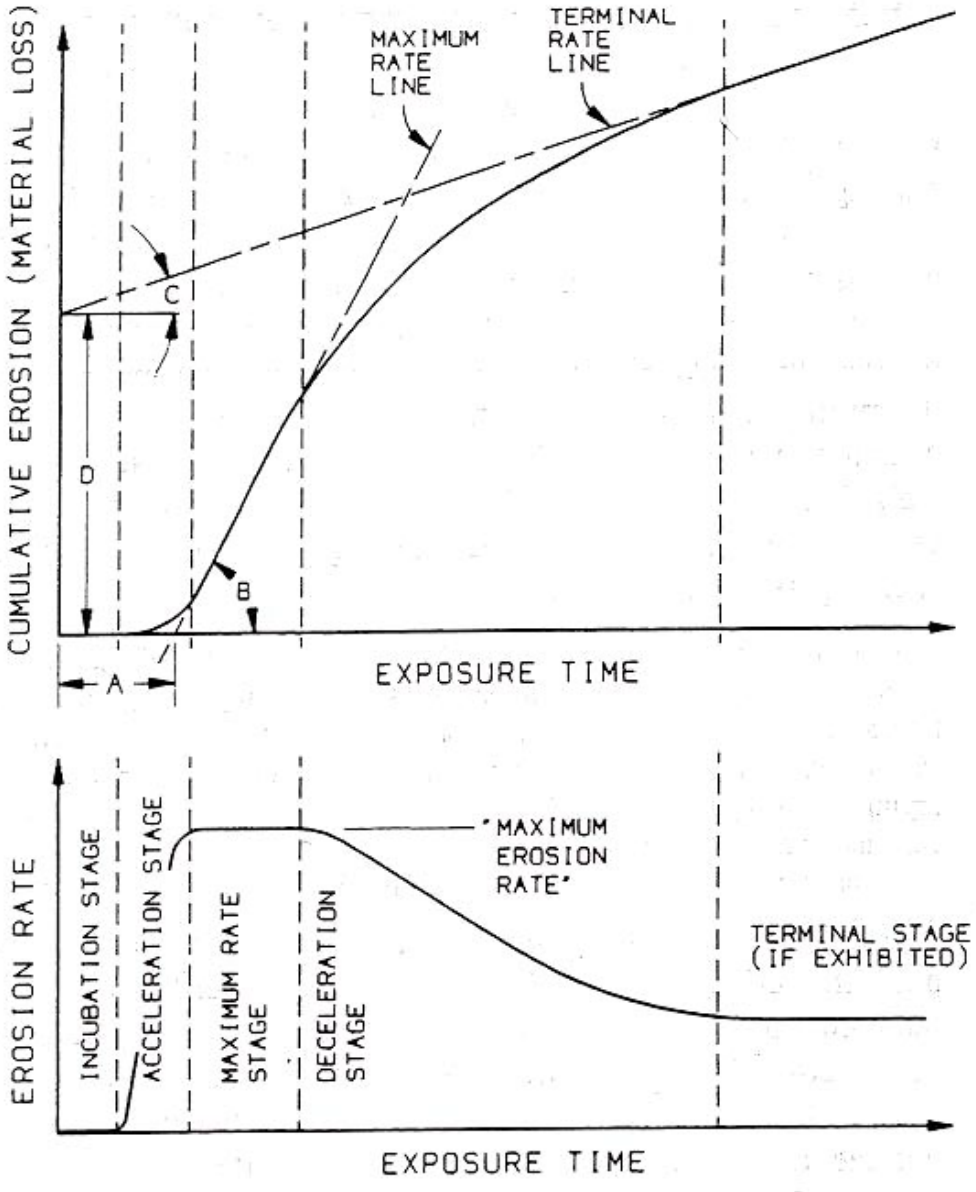

Fig. 23. Characteristic stages of erosion-time patterns in cavitation [20].

This pattern is derived from weight loss measurements and involves many pits at different stages of development. Growth of individual pits seems to be sporadic and unpredictable Interpretations of the various stages are:

- Incubation; surface hardening and initiation of first pits.
- Acceleration; expansion of damage over the whole area of the specimen.
- Maximum rate; steady state rate on uniformly damaged surface.
- Terminal; reduced rate of damage due to cushioning effects of liquid trapped in pits and crevices; deflection of jets by slopes on roughened surfaces.

The incubation period means that laboratory tests for screening materials for pitting resistance should be conducted to a high enough number of impacts to ensure that the rapid rate of pitting has been reached. It is important to remember that this pattern is for acoustic vibration and may not be applicable to other cavitation routes.

7.4 Materials rankings

Development of the acoustical testing technique allowed rapid comparative testing of materials for erosion resistance under standardized conditions and resulted in bar charts as shown in Fig. 24.

The data are normalized to annealed 300 series austenitic stainless steel, which is given an erosion rating of one. Compared to it, aluminum alloys have ratings <0.1. The most resistant materials, with ratings of 10 or more, are the cobalt-base Stellite alloys, tool steels, maraging steels, and ausformed steels that have been strain-transformed to martensite.

There is no well-defined correlation of pitting proclivity with physical or mechanical properties of the pitted material. In general, the greatest resistance to pitting is shown by those alloys that offer a combination of corrosion resistance, high strength (hardness), and toughness (but not hardness and brittleness). High strength for protection against pitting can be achieved throughout the bulk by cold working it or by heat treating prior to service. Or strength can be improved in just the surface layers before service by a surface hardening treatment such as carburizing, shot peening, or laser treatment, or by a surface coating treatment such as spraying, cladding (weld deposits), and plating. Effects of surface treatments are not included in Fig. 24. Surface hardening treatments generally affect only shallow depths of tens of microns. Surface coatings can be tens of millimeters thick, and are particularly useful for rebuilding eroded

surfaces. A shortcoming with shallow, one-time surface treatments, is that they can give a false sense of security. They may seem to offer satisfactory resistance in the short term, but once they are broken through, pitting might suddenly accelerate. Better alternatives to the one-time surface treatments are surface hardening treatments that are self-renewed during service by the hammering action of the pitting process. Such continuously renewed hardening depends on plastic strain caused in the surface layers by the impacts; the strain either work hardens the layers or causes them to transform to another, tougher phase, usually to a martensite phase. Alloys with low stacking fault energy, such as Stellite and prestrained stainless steels, are found to be suitable for these treatments [21]. From these considerations, it seems that maximum resistance to pitting in the long term will be offered either by bulk treatments or by surface hardening treatments that are continuously renewed by the cavitation action.

For many years there has been a search to find the best parameter or combination of parameters describing a material, which could serve as a reliable figure of merit for resistance to cavitation erosion. In general, there has been found no reliable parameter that can fully describe cavitation erosion resistance. One suggested metric is derived from examinations of the dependence upon the material hardness of the volume of individual particles eroded from the surface. This dependence is combined with dependence of the particle removal rate, which is taken to be proportional to the fatigue crack growth rate. The resulting erosion volume loss rate in the maximum rate stage (Fig. 23) is found to be proportional to $H^{-3/2}E^{-2}$, where H is Vickers hardness and E is Young's modulus [22]. This parameter gives a good correlation for Al, Cu, and carbon steel, in both annealed and hardened and tempered conditions over three orders of magnitude in erosion volume loss rate.

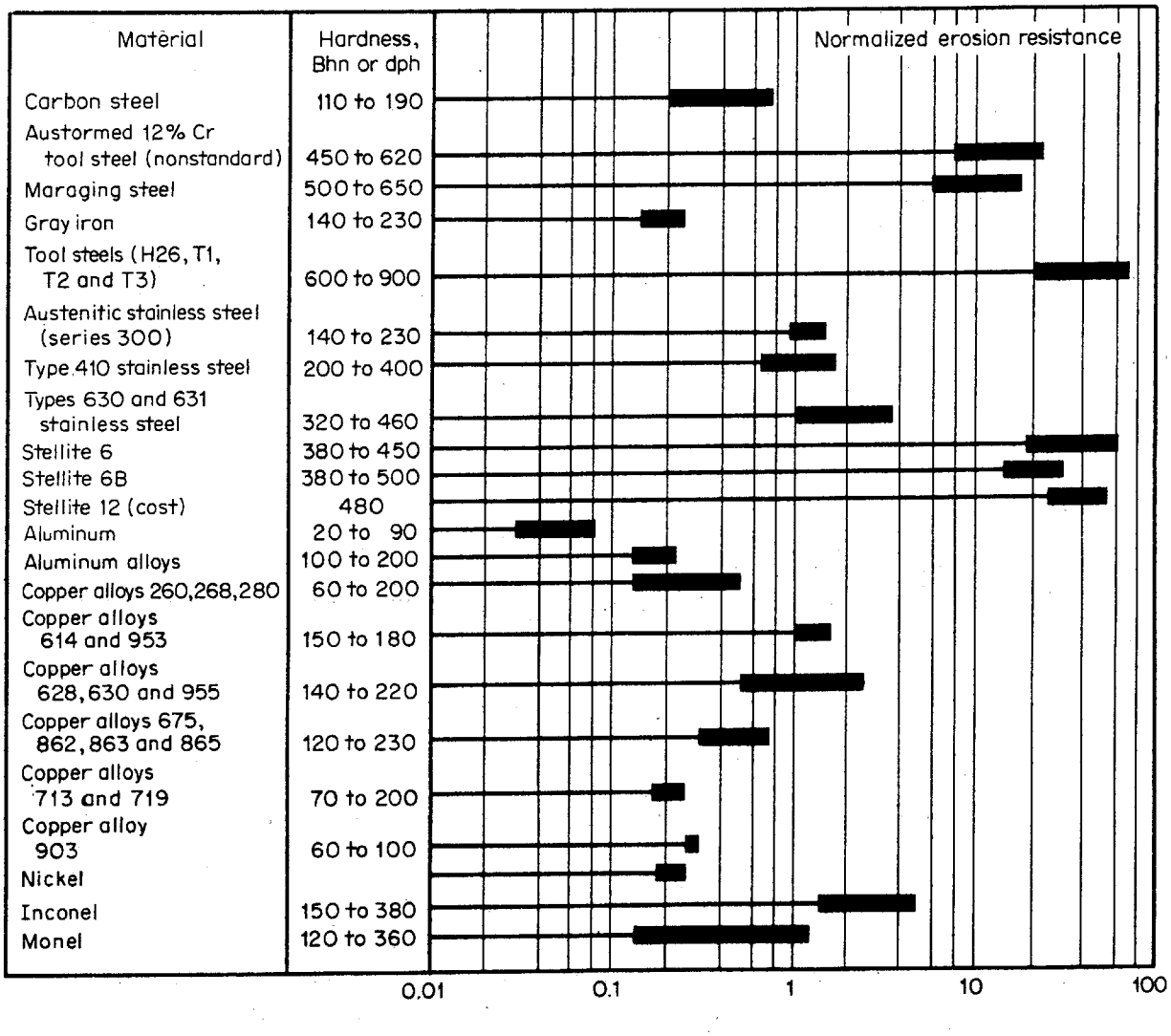

Fig. 24. Erosion resistances of various alloys relative to 18Cr-8Ni austenitic stainless steel [6].

7.5 Cavitation erosion in mercury

Cavitation in a liquid mercury target was broached as a likely possibility in the context of the SNS target based on an examination of design parameters and cavitation thresholds [16]. It was pointed out that cavitation erosion might or might not be a problem, depending upon whether cavitation bubbles formed close to the surface of the target container or in more distant regions.

Relatively little is known about cavitation erosion in liquid mercury, but several features are established. One is that pitting does occur in various types of tests [14][15][17][19]. Another is that the degree of pitting is decidedly worse, 3 to 20 times, than in water under similar test

conditions [14][15][17]. In examining the parameters relevant to the possibility of cavitation erosion in the SNS target it was found that a type 316 stainless steel exposed in water and mercury differed in its erosion response to increasing input power level in acoustic horn experiments [17]. In water the erosion depth exhibited a linear response to input power, while in mercury it exhibited a greater than linear response that could be approximated as a quadratic function. In later experiments for the SNS, an ultrasonic transducer was used to generate cavitation damage on specimens of annealed 316L stainless steel immersed in mercury [18]. In a 24 h exposure, tenacious mercury wetting of the stainless steel was developed and, after cleaning, the specimen was found to be significantly roughened in uniform fashion over all exposed surfaces (no isolated pits). SEM profile analysis indicated peak-to-valley surface roughness of at least 15 μm on the eroded specimen compared to 0.5 μm on the virgin specimen.

At the present time experiments are ongoing using an acoustic horn technique similar to that described in [20]. Initial testing has focused on the cavitation erosion of annealed 316LN in mercury at 25 °C to establish the specimen and test conditions required to generate reproducible results. It is evident from the preliminary information that the ultrasonic processor can be used to develop significant cavitation that results in relatively uniform surface roughening across the exposed specimen surface. To date, isolated pits have been observed infrequently, only for the longest exposure times and always accompanied by uniform erosion. Future tests will compare annealed 316LN with 316LN in other conditions, which include cold-worked, surface-modified or coated, and welded. Other alloys will be examined for comparison, as well as the effects of modifying test conditions over a limited range relevant to the SNS target, such as by varying test temperature. Results from this program will be used to rank the erosion resistance for materials of interest, to assess materials for potential inclusion in future in-beam tests, to interpret related test data, and to evaluate potential design modifications for the target container.

From the sparse data, it also seems that the erosion resistance rankings of materials in mercury at room temperature are similar to those in water at room temperature [14]. It was presumed [14] that the greater damage in mercury was due to the greater density of mercury, which is 13.5 times larger than water. But other differences in physical properties for mercury at room temperature are surface tension (6 times larger than water), bulk modulus (13x), viscosity (0.1x), specific heat (0.03x), thermal conductivity (15x), heat of vaporization (0.1x), thermal expansion (9x), compressibility (0.09x), and vapor pressure (0.0001x to 0.001x for temperatures

of interest). These properties will affect the formation and collapse parameters of cavities, and the pitting forces. For example, for a given amplitude pressure pulse in water and mercury, the damage would be expected to be worse for mercury because the compressibility is much lower and the surface tension is much larger. Lower compressibility means less cushioning of a blow to the boundary surface and higher surface tension means a more violent collapse of small bubbles.

7.6 Cavitation in TTF Feed lines

The SNS Target team accumulated some additional firsthand experience on the cavitation phenomenon during the final development tests on the full-scale hydraulic test loop referred to as the Target Test Facility (TTF). Cavitation occurred in the feedlines to the prototypical target just downstream of the second of two 90-degree bends spaced closely together. The onset of cavitation occurred at flow rates that were about 20% of the nominal value. When operated at the nominal flow rate, the system was extremely noisy, making audio communication outside the TTF enclosure difficult and causing significant vibration of the concrete floor in the building housing the experiment.

Prior to redesigning and replacing this section of feed line piping, the TTF loop was operated for several hours at nominal and one-half nominal flow rates to gather data on the velocity field in the prototypical target. It is worth noting that the ultrasonic Doppler velocimeter measurements were greatly facilitated by the presence of cavitation bubbles. Measurements could not be made on the previous TTF configuration because inadequate scattering surfaces existed in the flow.

Despite operating under these extremely noisy conditions for hours, it is remarkable that no significant damage to the feedline piping could be detected in the post-mortem examination of the section of piping where the noise originated. However, it should be noted that no pre-inspection of the piping surface was performed, so that minor changes of the surface would not have been detectable. These results lead one to speculate that flow induced cavitation of the type experienced in TTF is a very different phenomenon than the cavitation that is occurring in targets exposed to short pulse proton beams where significant damage occurred in a very short period of exposure to the cavitation environment.

8.0 Mitigation Strategies

It should be pointed out that there might be an automatic mitigation process operating for the SNS target. It is known that displacement-inducing irradiation causes substantial hardening in structural materials. Typically, for irradiation of solution annealed austenitic stainless steels the yield strength increases by a factor of two to three after irradiation to doses of only 0.01 to 0.1 dpa, i.e., 0.1 to 1 day at the front center of the target at full power. Hardening is generally found to be beneficial in reducing cavitation erosion. In this respect cold-worked materials, which provide some qualitative similarities in hardening to irradiated materials, will be tested in the ongoing experiments described in section 7.5.

An option that has yet to be investigated is textured surfaces. There are qualitative arguments to suggest that such an approach might result in reducing erosion. Textured surfaces can be produced by etching, hammering, shot peening, milling, or rolling, the latter two being reproducible. The size scale of the texturing might have to be of the size of pits, say 100 μm or so. A suggestion that this approach might be effective can be gleaned from Fig. 23. There the deceleration and lower steady-state terminal stage of erosion are associated with highly textured surfaces (where the processing route for obtaining the textured surface is cavitation erosion.)

Other concepts for potentially mitigating cavitation erosion in mercury include:

- Entrain gas bubbles to reduce the formation of vapor bubbles and increase macroscopic compressibility.
- Reduce surface energy of mercury (Composition or thermodynamic external variable change required to alter a physical property).
- Insert “steel wool” or other mesh-like material in Hg to break up/scatter pressure waves.

All of these concepts would require considerable experimental verification.

9.0 Plans for near-term testing

Five testing activities that could contribute to our understanding of the pitting phenomenon will be undertaken before the end of FY 2002, including:

- Additional rounds of in-beam tests at LANL's Weapons Neutron Research (WNR) facility,
- Another round of in-beam tests at BNL's Alternating Gradient Synchrotron (AGS) facility under the auspices of the AGS Spallation Target Experiment (ASTE) collaboration,
- Off-line mechanical load tests on cylindrical (LE) targets to benchmark computer simulation models,
- Off-line tests using JAERI's split Hopkinson pressure bar (SHPB) apparatus to determine the pressure threshold for pitting damage, and
- Cavitation damage tests using an ultrasonic processor to perform screening/comparison tests of target container material candidates.

The test program for each element listed above is briefly described below.

9.1 WNR

We plan to conduct one more round of mercury target tests at LANL's WNR facility. A proposal for five days of beam time was recently submitted, and the proposal review committee will meet in April to select those projects that will be given beam time during this year's LANSCE operating schedule that runs from July 1 to December 24. We have requested that our tests be scheduled as early as possible. Although a WNR pulse contains less energy than a pulse for the 2 MW SNS, by focusing the WNR beam down to a size of about 20 mm diameter, the beam intensity, and therefore pressure increase, expected for the SNS can be reasonably simulated. Tests conducted during 2001 are discussed in a previous section of this paper.

Having determined in last year's tests that pitting can occur under pulsed beam conditions, the main purpose of the new tests is to address the following four issues:

(1) Does a small void at the top of the target eliminate or greatly reduce pitting,

(2) Is there a threshold for pitting that is a significant fraction of the full-power intensity of SNS, say 25% or more,

(3) Can the use of more prototypical shaped targets reduce or eliminate pitting,

(4) Can the use of more cavitation damage resistant materials reduce or eliminate pitting?

Item (1) is motivated by the results obtained in the December 2001 tests with Pb-Bi. The strains were anomalously low for this target, and post-test examination of the target indicates that a small void, approximately 1% by volume, likely existed. Item (2) could establish whether a mercury target in SNS might not experience significant pitting damage during the initial few years of operation where low powers are expected. This would allow significant time to develop solutions to the pitting problem in the real SNS environment. Item (3) is motivated by conjecture that the large pits formed in previous tests were primarily due to the radial focusing of pressure waves in an axi-symmetric target. Item (4) is based on the potential for improvements already demonstrated in hardened samples used in previous WNR tests. Since both items (3) and (4) were studied in December 2001, specification of detailed designs and material specimens will await inspection of these test samples.

The surface of the flanges exposed to the mercury will be carefully characterized and micrographed prior to and following tests. A series of single-pulse tests will be conducted on these targets with the total number of pulses limited by the activation and operational limits for experiments in the WNR Blue Room.

9.2 ASTE

A series of tests will be conducted at BNL's AGS facility in May on four LE targets being built by our collaborators from FzJ. The ESS team will use the four front diaphragms on these cylindrical targets to test their baseline ferritic steel material, while the SNS team will use the rear diaphragms to study methods to mitigate pitting damage. The heating conditions, and therefore magnitude of the pressure pulse, are essentially the same on the front and rear of these 300 mm long targets. The two pitting mitigation methods to be examined in these tests are the use of hard, cavitation damage resistant coatings and the use of a small void at the top of the target. A bare 316SS diaphragm will be used on one target as a control sample to demonstrate that pitting damage conditions are achieved under the planned beam conditions of 3×10^{12} protons per pulse, 24 GeV protons, and 200 pulses for each target. Another bare stainless steel diaphragm will be used for the target with a small void at the top. The two other diaphragms will be coated with either CrN or a non-crystalline metallic glass coating that was recently developed at the Idaho National Engineering and Environmental Laboratory (INEEL) [23]. The JAERI

team is providing the CrN coating, while the SNS team is arranging for the metallic glass coating.

9.3 Mechanical testing of LE targets

To improve our understanding of the response of the test targets and benchmark our computer models being used to predict the response of the SNS target to pressure pulses, we plan to conduct a series of simple mechanical load tests on an LE target. The LE target, which will be struck with a "calibrated" hammer to impose a dynamic load, will be instrumented with fiber-optic strain gauges. Tests will be conducted with the target empty, filled with water, and filled with mercury. In each case, predictions from ABAQUS computer models of the target will be compared with the measurements. Given that the level of the mechanical load may not be highly repeatable, achieving the correct frequency response is of primary importance in this comparison between predictions and measurements. Models will be adjusted, if necessary, to achieve the desired level of agreement.

9.4 SHPB

Previous tests on JAERI's split Hopkinson pressure bar were conducted at two pressure levels that are consistent with proton beam power levels of about 2 MW and 4 MW on SNS. Researchers at JAERI have agreed to conduct additional tests at pressure pulse levels that are lower than this range to investigate whether the threshold for pitting damage might allow us to operate at significant, but reduced, power levels, without encountering this phenomenon. For example, the JAERI team will perform their tests at the equivalent of 1 MW operation (pressure pulse of 20 MPa). If damage still occurs at this level, they will reduce the pressure level again, say to 10 MPa, and conduct more tests.

9.5 Ultrasonic processor

An ultrasonic processor (e.g., a vibratory horn) produces cavitation damage on the face of a test specimen being vibrated at high frequency (20 kHz) while immersed in the test fluid (mercury or water). The rapid reciprocating displacement of the specimen surface induces the formation and collapse of cavities in the liquid, and the collapsing cavities are capable of producing damage on the specimen surface that can be quantified by weight loss and/or

penetration depth as a function of exposure time. The basic test protocol and equipment is described by ASTM Standard G-32 and, provided critical parameters are controlled from test-to-test, this procedure permits qualitative or semi-quantitative comparison of damage rates for a wide variety of materials/treatments.

Presently, there is no specific correlation between the damage intensity/rate produced at the surface of the specimen in the vibratory horn and potential cavitation damage in the SNS mercury target containment resulting from proton pulses. As a result, data from the vibratory horn tests cannot be used to quantitatively predict target life. However, testing can assess relative cavitation resistance of annealed 316LN (the reference material) compared to 316LN in other conditions (e.g., cold worked, surface treated) and other alloys with potentially superior cavitation resistance. Temperature, displacement amplitude, and exposure time are expected to be significant variables for consideration in the test exposures and should be fixed in order to provide valid comparisons. Ultimately, results from this screening test will be used to select appropriate materials for the next round of examinations at the WNR.

10.0 Pitting Erosion Lifetime Estimates

Estimating the target lifetime using the data from the 200 pulse tests requires an enormous extrapolation. The nominal target lifetime based on embrittlement due to irradiation damage is set at 1250 hours for a pulse repetition rate of 60 Hz and time averaged power of 2 MW (corresponds to 5 dpa in 316SS). This goal represents 2.7 x 10^8 pulses, or more than a factor of a million more pulses than obtained in the tests. Nonetheless, extrapolation is judged to be worthwhile to give some comparison of projected lifetimes with design goals.

The images showing pits from the July 2001 tests were used to estimate the fraction of area that was damaged and the depth of the damage. Estimates were made for both types of pits observed in these tests, i.e. large pits clustered near the center and smaller pits distributed randomly in clusters at a few locations on the surface of the flange. In all cases, we used data from the worst regions of pits and assumed this damage occurred everywhere on the surface. This could be significantly conservative for the small pits, but is likely more realistic for the large pits, which appear to collect near the beam interaction zone (perhaps rotated 180 degrees around the center of the diaphragm).

Key assumptions used for this extrapolation include:

- Damage from WNR pulses with stagnant Hg target is the same as SNS damage, i.e. assumes energy density and ratio of beam to target cross-section are the critical parameters,
- Pitting damage remains constant (same amount of material is removed even after the surface is heavily pitted) at the value measured in the small number of test pulses,
- The thickness of material available for erosion is 500 μm.

By examining the SEM images in the damaged regions, we estimated the pit density (n_p = pits per unit area) and the characteristic diameter of the pits (d_p). Using this data, the fraction of the surface area that is damaged (f) is given by:

$$f = n_p \frac{\pi}{4} d_p^2$$

The number of pulses that would be required to remove one layer of material is:

$$\frac{N_T}{f} = \frac{4\, N_T}{\pi\, n_p\, d_p^2}$$

where N_T is the number of pulses in the test (200 for the July 2001 tests). The number of layers until end-of-life is reached is simply the thickness (t_L) of material available for erosion (assumed to be 0.5 mm for our case) divided by the characteristic depth (h_p) of the pits. Assuming that the characteristic pit depth is equal to one-half the characteristic diameter, then the number of pulses in the lifetime (N_L) is estimated to be:

$$N_L = \frac{8\, N_T\, t_L}{\pi\, n_p\, d_p^3}$$

The target lifetimes estimated using this linear extrapolation from the test data are shown parametrically in Fig. 25 for pit diameters ranging from 4 to 100 μm. Four data points, corresponding to large and small pits for the bare annealed and treated (Kolsterised) diaphragms, are displayed in this figure.

It is obvious from these extrapolations that the large pits will lead to unacceptably short lifetimes on either bare or Kolsterised 316SS surfaces. Therefore, it is clear that some means must be found to eliminate the large pits.

The estimated lifetimes due to erosion from randomly distributed clusters of small pits are roughly three orders of magnitude greater than those for large pits. The bare 316SS would be expected to last about 6 x 10^6 pulses, or about 30 hours at full power with a repetition rate of 60 Hz. For purposes of estimating the potential lifetime that might be possible, the Kolsterised surface is assumed to extend to 500 microns, whereas it is actually only 33 microns thick. The lifetime of such a material would be estimated to be about 10^8 cycles or within roughly a factor of three of the desired value.

Lifetime goals for early phases of SNS operation are also indicated on Fig. 25 to illustrate that the lifetime goal for the first several years of operations are significantly relaxed compared to the ultimate goal of 1250 hours at 2 MW. If the extrapolation performed here applies and large pits are eliminated by geometric or other considerations, bare 316SS should be adequate for the first six months of operations with no target replacement.

It must be emphasized that results from this extrapolation exercise have huge uncertainty bands. Important questions that have yet to be answered include

- Is there an incubation period, i.e. does the erosion actually increase after some initial period of cycles?
- Does hardening of the surface by pitting damage or irradiation slow down the pitting?

- Should the damage fraction be averaged over the entire diaphragm surface?

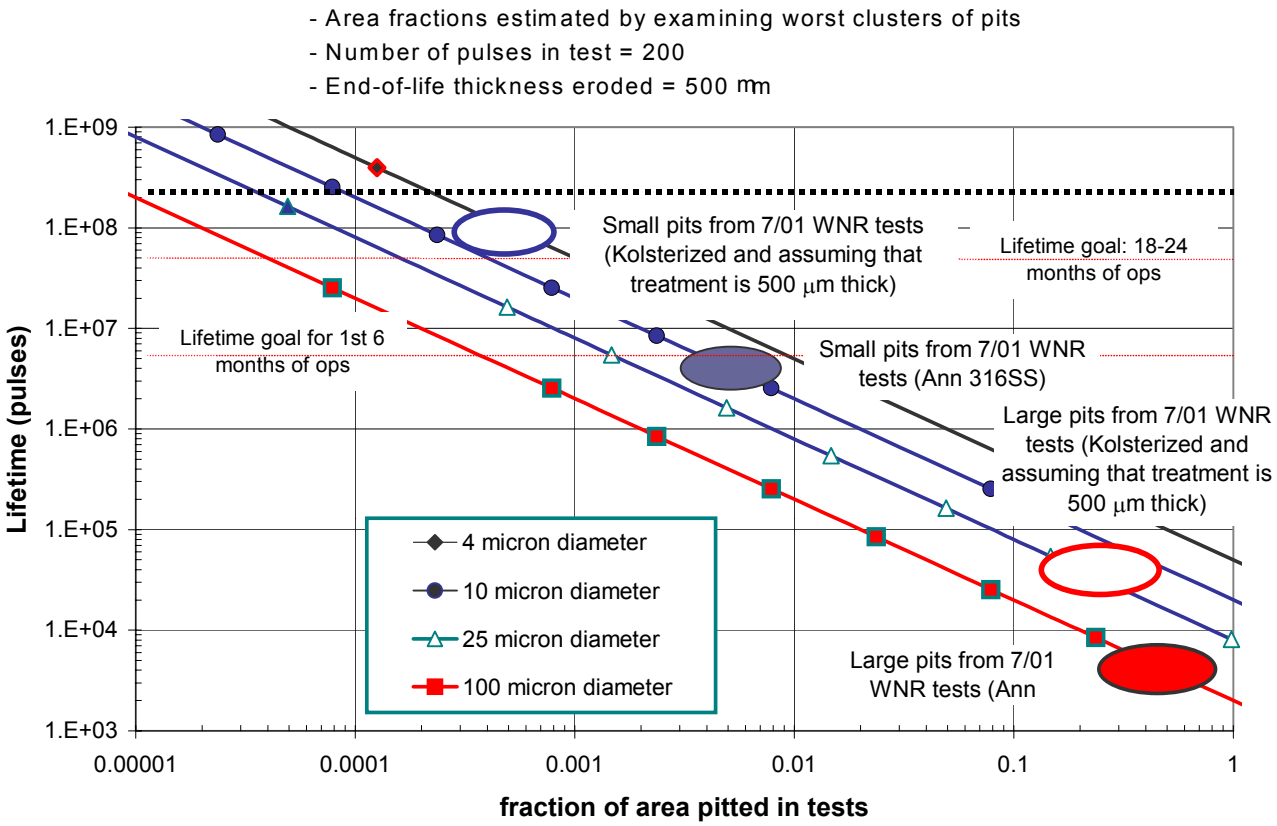

Fig. 25. Target lifetime estimates extrapolated from WNR test results.

11.0 Concluding Remarks

A series of tests were conducted at LANL's WNR facility during 2001 to examine whether the pressure pulse phenomenon caused by the interaction of a short-pulse (300 ns), high-energy proton beam with mercury causes pitting damage to the stainless steel container. Results showed that, at least for the materials and target configurations tested, pitting damage occurred. A cluster of large pits, visible to the naked eye, as well as smaller, more randomly distributed pits were seen in micrograph images of all four window specimens used in the July 2001 tests.

Subsequent tests at the WNR in December 2001 were dedicated to further examining the pitting phenomenon and looking at an array of possible solutions, or at least reductions, to the pitting problem. Seven targets were tested in the December 2001 campaign. Most notably, a target with a rectangular cross section was used in an attempt to eliminate the postulated radial focusing of the pressure wave and be more prototypical of the actual SNS target shape. Also, windows with increased thickness, intended to reduce the large stresses, were tested. Post-irradiation examination of the targets irradiated in December has begun and is scheduled for completion in April 2002.

The magnitude of the pressure pulse, results of off-line cavitation threshold tests, and post-test examination of damaged surfaces, lead us to conclude with a reasonably large degree of confidence that the mechanism causing the pitting damage is collapse of bubbles created as part of a mercury cavitation process. Because of this, the cavitation damage literature has been studied to help understand the phenomenon and postulate potential solutions or improvements.

To date, in-beam tests have not been able to clearly demonstrate a solution to the pitting issue, although a couple of concepts/material combinations may hold promise. One concept is the use of a non-axisymmetric shaped target, which is more prototypical of the SNS target shape, with either no double wall structure near its front or using water in this thin slot formed by the double wall. Either of these changes represent a modification to the SNS baseline design and will require careful evaluation before they could be incorporated, and may lead to breakage of engineering design, increased component costs, and greatly reduce or even eliminate all schedule float in SNS target fabrication, installation, and testing.

The use of more cavitation damage resistant materials may also offer improved erosion lifetime performance, but will certainly increase the unknowns relative to behavior under irradiation. The irradiation database developed for 316SS under relevant spallation target

conditions has given us great confidence in projecting minimum lifetimes and minimizing risk of premature target failure during SNS target operation. This increased uncertainty must be given consideration in making a decision to switch to a different target container material.

Estimating the target lifetime using the data from the 200 pulse tests requires an enormous extrapolation, i.e., by more than a factor of one million. Assumptions regarding the nature of the pitting process that have yet to be validated are required to create this erosion lifetime estimate. Nonetheless, extrapolation is judged to be worthwhile to give some comparison of projected lifetimes with design goals. These estimates illustrate that the large cluster of pits near the center of the beam interaction region must be eliminated to achieve adequate lifetimes. If the large pits are eliminated by geometric or other considerations (not fully demonstrated yet), bare 316SS should be adequate for the first six months of operations with no target replacement. If we can find a target container material that has an erosion resistance comparable to that of the Kolsterised surface (limited to 33 μm thickness) over an erosion thickness greater than 500 μm, then lifetimes approaching 1/3 of the goal at 2 MW operation may be possible. This would give us adequate target lifetimes for several years of operation, which could presumably be used to examine methods to further extend the erosion lifetime.

Finally, the direct relevance of the off-line and in-beam tests conducted so far is somewhat questionable since many of the conditions/variables that could be important for pitting damage cannot be accurately simulated in these tests. Several examples of the discrepancies between tests and the actual SNS conditions include:

- Interactions between subsequent beam pulses could be important if the residence time of cavitation bubbles is comparable to or longer than the 17 ms between pulses in SNS (corresponds to 60 Hz repetition rate),
- Flowing of the mercury may alter the contact condition between the mercury and stainless steel and thereby change the way in which bubbles form and collapse,
- The geometries used in tests have been either different or rather great simplifications of the SNS target shape, lacking structural details, and the long open-ended supply and return lines that flow the Hg, and
- Both off-line and in-beam tests have been limited to a small number of pulses (≤ 200) compared to the baseline target lifetime (based on radiation damage) of 3×10^8 pulses.

Given the uncertainty in erosion lifetime it is concluded that more in-beam tests be performed to examine whether the proposed ideas for target shape and materials can be shown to extrapolate to reasonable lifetimes (say 10^8 pulses for example) at SNS relevant power levels (≥ 1 MW). Tests are scheduled for June 2002, but additional tests may be required. Also, developing Hg target design concepts, diagnostics, and post-irradiation examination procedures that emphasize the experimental nature of early SNS operations should be pursued.

References:

[1] L. Briggs, "The Limiting Negative Pressure of Mercury in Pyrex Glass," Journal of Applied Physics, Vol. 24 (1), April 1953.

[2] F. Moraga and R. P. Taleyarkhan, "Static and Transient Cavitation Threshold Measurements for Mercury, Proc. of AccApp'99, November 1999.

[3] M. R. Cates, B. W. Riemer, D. D. Earl, C. C. Tsai, S. W. Allison, D. L. Beshears, J. R. Haines, "Strain Measurements on Targets Tested at the LANSCE WNR Facility," August 2000, SNS-101050200-TR0009-R00, July 12, 2001 (SNS/TSR-0215).

[4] Brennen, C. E., CAVITATION AND BUBBLE DYNAMICS, Oxford University Press, 1995.

[5] Lord Rayleigh, Phil. Mag. 34 (1917) 94-98.

[6] G. Hammitt, "Cavitation and Liquid Impact Erosion," pp. 161-230 in ASME Wear Control Handbook, pub. Amer. Soc. Mech. Eng. (1980).

[7] C. M. Hansson and I.L.H. Hansson, "Cavitation Erosion," pp 214-220 in ASM Handbook Vol 18, Friction, Lubrication, and Wear Technology, pub ASM International (1992).

[8] Karimi and J. L. Martin, Int. Metals Rev. 31 1-26 (1986).

[9] F. J. Heymann, "Liquid Impingement Erosion," pp 221-232 in ASM Handbook Vol 18, Friction, Lubrication, and Wear Technology, pub ASM International (1992).

[10] Y. Tomito and A. Shima, J. Fluid Mech. 169 535-564 (1986).

[11] Philipp and W. Lauterborn, J. Fluid Mech. 361 75-116 (1998).

[12] R. T. Knapp, J. W. Daily, F. G. Hammitt, *Cavitation*, McGraw-Hill, New York, New York, 1970.

[13] C.E. Brennen, *Cavitation and Bubble Dynamics,* Oxford University Press, Oxford, England (1995).

[14] R. Garcia, F. G. Hammitt, and R. E. Nystrom, pp 239-283 in Erosion by Cavitation or Impingement, ASTM STP 408, Am. Soc. Testing Mats. (1967).

[15] S. G. Young and J. R. Johnson, pp 186-219 in Erosion by Cavitation or Impingement, ASTM STP 408, Am. Soc. Testing Mats, (1967).

[16] D. West, pp 645-649 in AccApp '98, Proceedings of 2nd International Topical Meeting on Nuclear Applications in Accelerator Technology, Gatlinburg, TN, Sept. 20-23, Pub. Amer. Nucl. Soc. (1998).

[17] M. D. Kass, J. H. Whealton, N. E. Clapp Jr., J. R. Distefano, J. H. Devan, J. R. Haines, M. A. Akerman, and T. A. Gabriel, Tribology Letters 5 231-234 (1998).

[18] S. J. Pawel, E. T. Manneschmidt, R. P. Taleyarkhan, S. H. Kim, and J. R. DiStefano, "Cavitation as a Mechanism to Enhance Wetting in a Mercury Thermal Convection Loop," ORNL/TM-2001/086 (May 2001).

[19] M. Futakawa, H. Kogawa, Y. Midorikawa, R. Hino, H. Date, and H. Takeishi, "Impact Erosion on Interface Between Solid and Liquid Metals", presented at the International Symposium on Impact Engineering, Kumamoto, Japan (ISIE/4), July 2001. To be published in symposium proceedings.

[20] ASTM Standard Test Method for Cavitation Erosion Using Vibratory Apparatus, Designation G32-98. Annual Book of ASTM Standards (1998).

[21] R.Simoneau, P. Lambert, M. Simoneau, J.I. Dickson, and G. L'Esperance, pp 32-1 to 32-8 in Proceedings of the Seventh International Conference on Erosion by Liquid and Solid Impact, Cambridge, 7-10 Sept. 1987, pub. Cavendish Laboratory, Cambridge University, United Kingdom.

[22] S. Hattori and E. Nakao, Wear 249 839-845 (2002).

[23] D. J. Branagan, W. D. Swank, D. C. Haggard, and J. R. Fincke, "Wear-Resistant Amorphous and Nanocomposite Steel Coatings," Metallurgical and Materials Transactions A – Physical Metallurgy and Materials Science, 32 (10): 2615-2621 (October 2001).